AD-A061 181 STANFORD RESEARCH INST MENLO PARK CALIF F/G 11/9
VISCOELASTIC AND FAILURE PROPERTIES IN BIAXIAL AND UNIAXIAL TEN--ETC(U)
DEC 66 T L SMITH, J E FREDERICK AF 33(615)-3248
UNCLASSIFIED AFML -TR-65-356-PT-2 NL

1 OF 1
AD A061 181

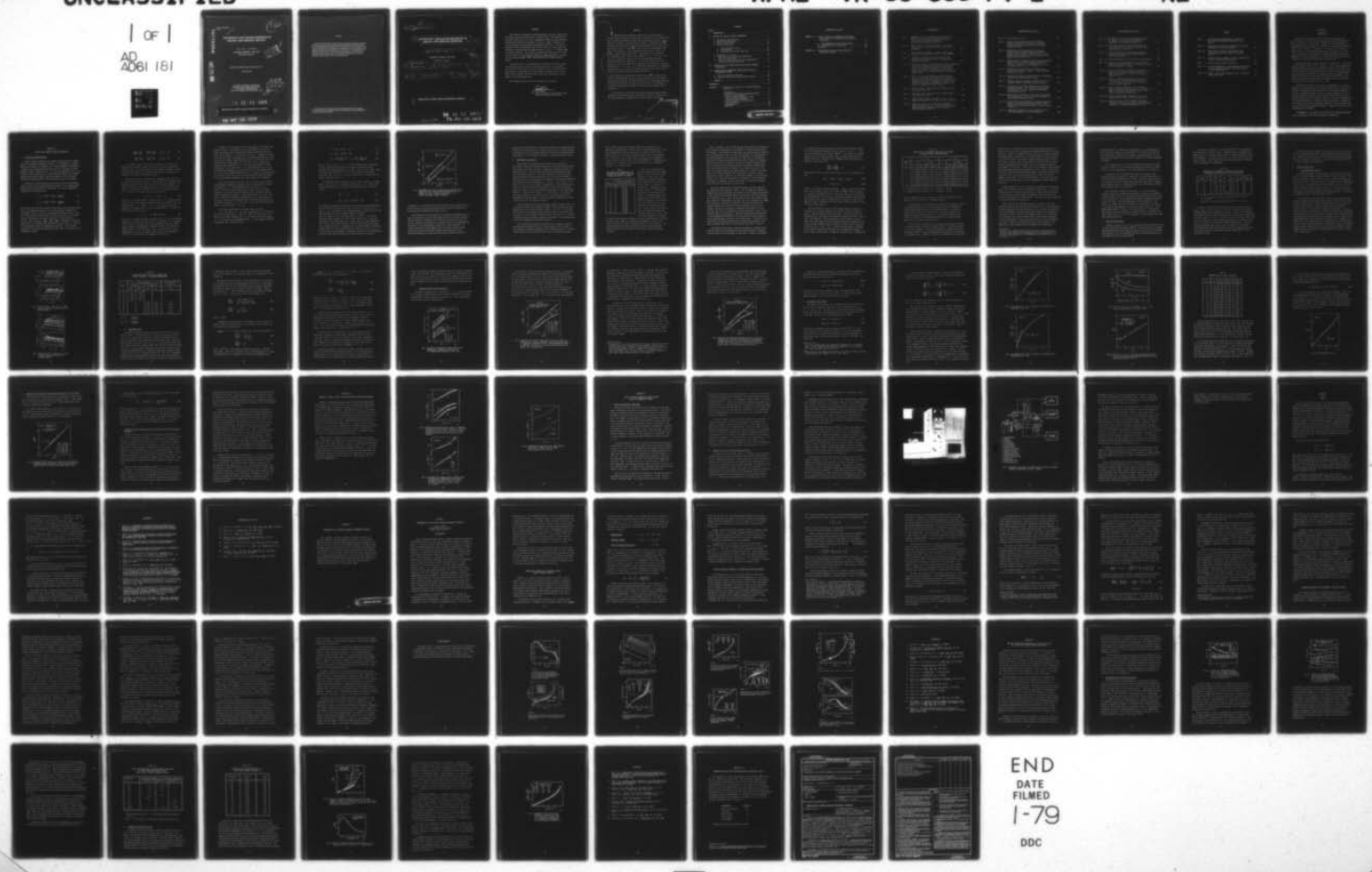

END
DATE FILMED
1-79
DDC

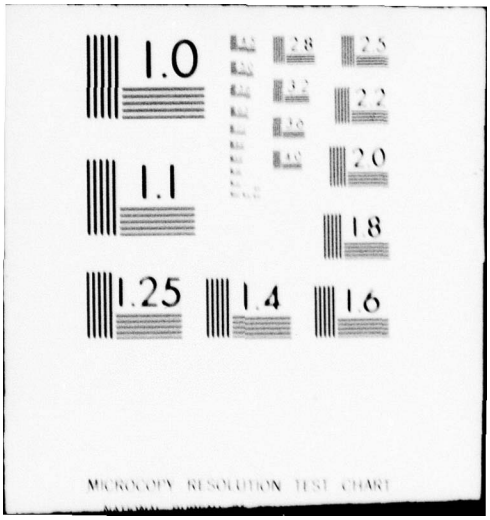
1.0
1.1
1.25
1.4
1.6
2.8
2.5
2.2
2.0
1.8
MICROCOPY RESOLUTION TEST CHART

AFML-TR-65-356
Part II

(1)2

VISCOELASTIC AND FAILURE PROPERTIES IN BIAXIAL AND UNIAXIAL TENSION

THOR L. SMITH J. E. FREDERICK

STANFORD RESEARCH INSTITUTE
Menlo Park, California

TECHNICAL REPORT AFML-TR-65-356, PART II

December 1966

AIR FORCE MATERIALS LABORATORY
RESEARCH AND TECHNOLOGY DIVISION
AIR FORCE SYSTEMS COMMAND
WRIGHT-PATTERSON AIR FORCE BASE, OHIO

NOTICES

When Government drawings, specifications, or other data are used for any purpose other than in connection with a definitely related Government procurement operation, the United States Government thereby incurs no responsibility nor any obligation whatsoever; and the fact that the Government may have formulated, furnished, or in any way supplied the said drawings, specifications, or other data, is not to be regarded by implication or otherwise as in any manner licensing the holder or any other person or corporation, or conveying any rights or permission to manufacture, use, or sell any patented invention that may in any way be related thereto.

Copies of this report should not be returned to the Research and Technology Division unless return is required by security considerations, contractual obligations, or notice on a specific document.

(19)

(18) AFML-TR-65-356 - PT - 2
Part II

(6) # VISCOELASTIC AND FAILURE PROPERTIES IN BIAXIAL AND UNIAXIAL TENSIONS, Part II.

(10) THOR L. SMITH J. E. FREDERICK

(11) Dec 66

(12) 192 P.

STANFORD RESEARCH INSTITUTE

Menlo Park, California

(9) Annual technical rept. 24 Aug 65 - 23 Aug 66,

(15) AF 33(615)-3248 (16) 7342 (17) 02

FOREWORD

This report was prepared by Stanford Research Institute, Menlo Park, California, under USAF Contract No. AF 33(615)-3248. The contract was initiated under Project No. 7342, "Fundamental Research on Macromolecular Materials and Lubrication Phenomena," Task No. 734202, "Studies on the Structure-Property Relationships of Polymeric Materials." The work was administered by the Nonmetallic Materials Division, Air Force Materials Laboratory, Research and Technology Division, with Mr. J. C. Halpin, MANE, as project scientist. This report, prepared under SRI Project No. 5724, covers the period from 24 August 1965 to 23 August 1966, and is released by the authors (December 1966) for publication as an AFML Technical Report.

The authors wish to acknowledge the contributions of James A. Rinde who, under the previous contract, designed the biaxial test equipment and carried out the tests at constant extension rates, of James R. Smith and Charles M. McCullough who are developing the apparatus for tests in equal biaxial tension, and of Richard L. Moore who assisted in certain phases of the experimental work.

This technical report has been reviewed and is approved.

J.M. KELBLE
Chief, Elastomers and Coatings Branch
Nonmetallic Materials Division

ABSTRACT

An unfilled styrene-butadiene vulcanizate was studied under a biaxial tensile deformation (essentially, pure shear) by stretching thin-wall cylindrical specimens axially while internal gas pressure was controlled to maintain a constant outside diameter. Between 25 and 90°C, specimens were stretched at crosshead speeds between 0.02 and 20 inches per minute; between -40 and 20°C, stress-relaxation measurements were made. From the data, at axial extension ratios λ_1 up to about 2.5, $W_1/G(t) \equiv (\partial W/\partial I_1)/G(t)$ and $W_2/G(t) \equiv (\partial W/\partial I_2)/G(t)$ were evaluated. W is analogous to the elastic stored energy; $I_1 = I_2 = \lambda_1^2 + \lambda_1^{-2} + 1$ are the strain invariants; and G(t) is the small-deformation stress-relaxation modulus in simple shear. It was found that $W_1/G(t)$ and $W_2/G(t)$ are time- and temperature-independent, that $W_1/G(t)$ is sensibly constant for $I_1 < 5.5$ (i.e., $\lambda_1 < 2.08$), and that $W_2/G(t)$ is a decreasing function of $I_1 = I_2$. From the results, uniaxial tensile data were calculated and found to agree with experimental data.

A comparison of rupture data between 25 and 90°C in biaxial and uniaxial tension showed that the ultimate extension ratios in biaxial and uniaxial tension are sensibly identical (at the same temperature and extension rate) but that the uniaxial rupture stress lies between the axial and circumferential rupture stresses under the biaxial tensile conditions.

A discussion is also given of the large deformation and ultimate properties of noncrystallizable vulcanizates in uniaxial tension and of the large deformation properties of a natural rubber vulcanizate.

CONTENTS

CONTENTS (Concluded)

ILLUSTRATIONS

ILLUSTRATIONS (Continued)

ILLUSTRATIONS (Concluded)

TABLES

SECTION I

INTRODUCTION

Studies of stress-strain behavior and ultimate properties in uniaxial tension of gum and filled vulcanizates have been described in previous reports.[1-4] In addition, a method[4] has been developed for obtaining data which represent the response to a pure shear deformation, namely, that for which $\lambda_1 = \lambda_3^{-1}$ and $\lambda_2 = 1.0$, where the λ's are the extension ratios in the mutually perpendicular directions. From such tests, rupture data were obtained on a styrene-butadiene vulcanizate (SBR-IV) at various extension rates at temperatures between 25 and 90°C; a preliminary discussion of these data has been given.[4]

This Annual Technical Report contains a discussion of: (1) biaxial tensile properties (specifically, response to a pure shear deformation) of SBR-IV under stress-relaxation conditions between -40 and 20°C, and both biaxial and uniaxial properties under conditions of constant extension rate between 25 and 90°C; (2) rupture properties of SBR-IV under biaxial and uniaxial tensile conditions between 25 and 90°C; and (3) current work directed toward obtaining stress-strain and rupture data under equal biaxial extension ($\lambda_1 = \lambda_2 = \lambda_3^{-\frac{1}{2}}$).

Supplementary material is presented in Appendices I, II, and III. Appendix I is a paper prepared for the Fall 1966 Meeting of the Division of Organic Coatings and Plastics Chemistry of the American Chemical Society. Although the paper is in part a review of past work, it contains new material on factors which affect the stress-strain curve in uniaxial tension and also it gives a comparison of the time dependence of the ultimate properties of different types of elastomers. Appendix II is devoted to the time and temperature dependence of stress-strain data for an unfilled natural rubber vulcanizate. Appendix III gives the compounding recipe for SBR-IV.

In Appendix I, the figures and references are numbered separately as are the figures, tables and references in Appendix II.

SECTION II

BIAXIAL AND UNIAXIAL TENSILE PROPERTIES

A. Theoretical Considerations

Biaxial tensile properties are currently being studied to explore facets of nonlinear viscoelastic behavior. The approach is to obtain data which represent the response of a typical amorphous vulcanizate to a simple type of mechanical excitation and then to develop a concise method for representing the data. To verify the general utility of the method for data representation, studies should be made of the response characteristics under several types of deformation fields and under multistep loading histories. Work along these lines is in progress.

Guidelines for data analysis are provided by Rivlin's[5] phenomenological theory for the large-deformation behavior of an incompressible material under equilibrium test conditions. For a pure homogeneous deformation, this theory gives:

$$\bar{\sigma}_1 - \bar{\sigma}_3 = 2(\lambda_1^2 - \lambda_3^2)(W_1 + \frac{1}{\lambda_1^2\lambda_3^2} W_2) \qquad (1)$$

$$\bar{\sigma}_2 - \bar{\sigma}_3 = 2(\lambda_2^2 - \lambda_3^2)(W_1 + \frac{1}{\lambda_2^2\lambda_3^2} W_2) \qquad (2)$$

where the $\bar{\sigma}$'s are the true stresses (stress based on the cross-sectional area of the deformed specimen) in the three mutually perpendicular directions, and the λ's are the corresponding extension ratios. Also, $W_1 \equiv \partial W/\partial I_1$ and $W_2 \equiv \partial W/\partial I_2$ where W is the stored elastic (or strain) energy, a function of the strain invariants I_1 and I_2 which are $I_1 = \lambda_1^2 + \lambda_2^2 + \lambda_3^2$ and $I_2 = \lambda_1^2\lambda_2^2 + \lambda_1^2\lambda_3^2 + \lambda_2^2\lambda_3^2$. Since Eqs. (1) and (2) apply only to an incompressible material for which $\lambda_1\lambda_2\lambda_3 = 1$, only two of the extension ratios are independent quantities. To facilitate evaluation of W_1 and W_2 from experimental data, Eqs. (1) and (2) can be rearranged to give:[4]

$$\frac{\lambda_1^2(\bar{\sigma}_1 - \bar{\sigma}_3)}{(\lambda_1^2 - \lambda_3^2)} - \frac{\lambda_2^2(\bar{\sigma}_2 - \bar{\sigma}_3)}{(\lambda_2^2 - \lambda_3^2)} = 2W_1(\lambda_1^2 - \lambda_2^2) \qquad (3)$$

$$\frac{(\bar{\sigma}_2 - \bar{\sigma}_3)}{(\lambda_2^2 - \lambda_3^2)} - \frac{(\bar{\sigma}_1 - \bar{\sigma}_3)}{(\lambda_1^2 - \lambda_3^2)} = 2W_2(\lambda_1^2 - \lambda_2^2) \qquad (4)$$

If W_1 and W_2, which in general are functions of I_1 and I_2, are known for all attainable values of I_1 and I_2, then the equilibrium response to any type of deformation can be computed. However, to determine W_1 and W_2 completely, data must be obtained which represent the response to a variety of deformation fields.

Relatively little is known about the dependence of W_1 and W_2 on I_1 and I_2 and on network structure. Extensive data on a natural rubber vulcanizate were obtained some years ago by Rivlin and Saunders.[6] In light of these data, they suggested that W_1 is sensibly constant and that W_2 is essentially independent of I_1 but is a decreasing function of I_2. That is, the strain energy W can be written:

$$W = W_1(I_1 - 3) + \Phi(I_2 - 3) \qquad (5)$$

where W_1 is a constant and Φ is a function only of I_2. Equation (5) is written in this form because W equals zero when the material is in its undeformed state, i.e., when $I_1 = I_2 = 3$. The data of Rivlin and Saunders[6] also suggest that, to a first approximation, $W_2 = 3W_2^o/I_2$ and thus that the strain energy is:

$$W = W_1(I_1 - 3) + 3W_2^o \ln(I_2/3) \qquad (6)$$

where W_2^o is a constant which may be considered to be either an adjustable parameter or the value attained by W_2 as I_2 approaches 3.0. This equation for the strain energy function was proposed by Gent and Thomas[7] largely because its mathematical simplicity expedites the solution of various types of elastic problems. If W_1 is a function of I_1 but is independent of I_2, then the strain energy is given by an expression like Eq. (5) except that W_1 now becomes a function of I_1.

In addition to the results of Rivlin and Saunders, data have been reported recently by Hutchinson, Becker, and Landel[8] for a natural rubber vulcanizate and a polydimethyl siloxane vulcanizate which contained 28% by weight of a reinforcing SiO_2 filler. Although their data on the natural rubber vulcanizate were in essential agreement with those of Rivlin and Saunders, Becker[9] has pointed out that the data cannot be represented in a simple manner in terms of W_1 and W_2, especially at relatively small deformation. For the filled polydimethyl siloxane vulcanizate, it was found that W_1 is an increasing function of I_1 and is essentially independent of I_2, and that W_2 is a decreasing function of I_2 and is also somewhat dependent on I_1. Finally, the characteristics of the strain energy function for a polyurethane elastomer (Solithane 113) at quite small deformations have been examined by San Miguel.[10]

If Eq. (5) is known to be valid, then W_1 and W_2 can be evaluated from data which represent the behavior of the material under one type of deformation, e.g., pure homogeneous shear for which $I_1 = I_2$. However, tests are required which give at least two of the normal stresses as a function of the deformation state; otherwise W_1 and W_2 cannot be separately evaluated. To determine whether or not Eq. (5) is valid, tests must be made which provide data over extended ranges of I_1 and I_2. Thus far in the present study, tests have been made only in pure shear for which $I_1 = I_2 = \lambda_1^2 + \lambda_1^{-2} + 1$ and in uniaxial tension for which $I_1 = \lambda_1^2 + 2\lambda_1^{-1}$ and $I_2 = \lambda_1^{-2} + 2\lambda_1$

A pure shear deformation is defined as that for which $\lambda_2 = 1$, $\lambda_3 = \lambda_1^{-1}$, and $\bar{\sigma}_3 = 0$. For such a deformation, the linear theory of elasticity shows that $\bar{\sigma}_1 = 4G\epsilon_1$, $\bar{\sigma}_2 = 2G\epsilon_1$, and thus $\bar{\sigma}_1/\bar{\sigma}_2 = 2.0$, where G is the shear modulus and ϵ_1 is the Cauchy strain which equals $\lambda_1 - 1$ in the limit as λ_1 approaches unity. For pure shear under large deformation, Eqs. (1) and (2) give:

$$\bar{\sigma}_1 = 2(W_1 + W_2)(\lambda_1^2 - \lambda_1^{-2}) \tag{7}$$

$$\bar{\sigma}_2 = 2(W_1 + \lambda_1^2 W_2)(1 - \lambda_1^{-2}) \tag{8}$$

$$\frac{\bar{\sigma}_1}{\bar{\sigma}_2} = \frac{(\lambda_1^2 + 1)(1 + \alpha)}{1 + \lambda_1^2\alpha} = 2 + \frac{(\lambda_1^2 - 1)(1 - \alpha)}{(1 + \lambda_1^2\alpha)} \tag{9}$$

where $\alpha \equiv W_2/W_1$. When $\epsilon_1 = \lambda_1 - 1$ is substituted in Eqs. (7) and (8) and only terms which contribute in the limit of small strain are retained, the following results: $\bar{\sigma}_1 = 8(W_1 + W_2)\epsilon_1$ and $\bar{\sigma}_2 = 4(W_1 + W_2)\epsilon_1$. This result shows that $2(W_1 + W_2) = G$ in the limit of zero strain. According to Eq. (9), $\bar{\sigma}_1/\bar{\sigma}_2 = 2$ only at small strains, except under the special conditions that $\alpha = 1$.

To illustrate the way in which $\bar{\sigma}_1$ and $\bar{\sigma}_2$ may vary with λ_1, we shall assume that W_1 and W_2 are constants and that $W_2/W_1 = 0.3$. Under these conditions (chosen only for illustrative purposes), Eqs. (7) and (8) become:

$$\frac{\bar{\sigma}_1}{G} = \lambda_1^2 - \lambda_1^{-2} \tag{10}$$

$$\frac{\bar{\sigma}_2}{G} = \frac{1}{1.3}(1 + 0.3\lambda_1^2)(1 - \lambda_1^{-2}) \tag{11}$$

To indicate the nonlinear deformation characteristics, data representing Eqs. (10) and (11) are plotted in Fig. 1 as $\log \bar{\sigma}_1/G$ and $\log \bar{\sigma}_2/G$ vs $\log (\lambda_1 - 1)$. According to the preceding discussion, data at sufficiently small deformations (linear response range) are given by $\log \bar{\sigma}_1/G = \log (\lambda_1 - 1) + \log 4$ and $\log \bar{\sigma}_2/G = \log (\lambda_1 - 1) + \log 2$; these equations represent the lines of unit slope in Fig. 1 which are separated by 0.30 logarithmic unit. Because the curves which represent Eqs. (10) and (11) become coincident with the lines of unit slope only at very small strains, it is apparent that G cannot normally be evaluated reliably from the initial linear portion of plots of $\bar{\sigma}_1$ or $\bar{\sigma}_2$ vs $\lambda_1 - 1$. (This situation arises because of experimental difficulties in maintaining precisely a pure shear deformation at small extension.) For most

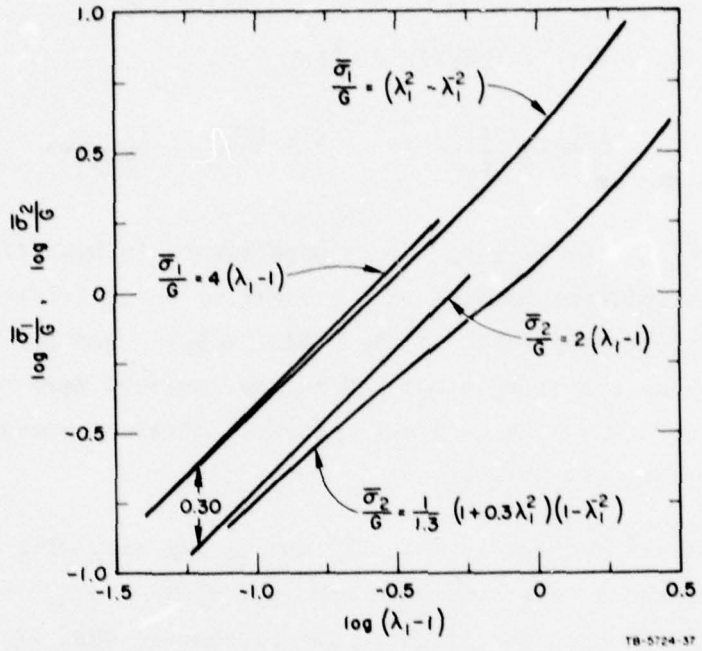

FIG. 1 DEPENDENCE OF LOG $\bar{\sigma}_1/G$ AND LOG $\bar{\sigma}_2/G$ ON LOG (λ_1-1) PREDICTED FOR A PURE SHEAR DEFORMATION BY THE THEORY OF FINITE ELASTICITY WHEN $W_2/W_1 = 0.3$ AND BY CLASSICAL LINEAR ELASTICITY

elastomers, it is expected that W_2 will decrease with an increase in λ_1; thus the deviation from linearity may occur at smaller extensions and may become more pronounced than shown in Fig. 1.

The method used in this report for analyzing time-dependent data is based on the theory of finite equilibrium elasticity with the exception that W_1 and W_2 are considered to be functions of time as well as of I_1 and I_2. As shown in Section II-E, either W_1 or W_2 can be represented by the product of a time-dependent function and a strain function. A critical evaluation of the general utility of these relations would require that tests be made under complex loading histories (e.g., multistep relaxation or creep tests) and that a nonlinear theory be

applied to determine whether the observed response can be predicted from the data given in this report. Theories which involve a single integral representation of time-dependent mechanical response data and which have been applied to data in uniaxial tension are discussed in Refs. 11-13.

B. Experimental Procedures

The method[4] for obtaining biaxial tensile data consists of stretching a thin-wall cylindrical specimen in the axial direction while gas pressure inside the specimen is regulated to maintain constant its outside diameter. The axial load and deformation are measured along with the internal pressure. From these quantities, the three normal stresses and the associated extension ratios on either the inside or outside surface of the cylinder can be computed, as discussed previously.[4] The extension ratios are defined by $\lambda_1 = L/L_o, \lambda_2 = C/C_o$, and $\lambda_3 = t/t_o$, where L, C, and t are the length, circumference (at some location on or within the specimen's wall), and thickness of the stretched specimen and L_o, C_o, and t_o are the corresponding quantities for the unstretched specimen. On the outside surface, $\lambda_2 = 1$ and thus $\lambda_1 = \lambda_3^{-1}$. Except on the outside surface, λ_2 is slightly greater than unity and thus the deformation is not pure shear, strictly speaking, although the deviation is quite small for the specimens studied.

To characterize partially the nonlinear response characteristics of the styrene-butadiene gum vulcanizate SBR-IV, biaxial tensile data were obtained from: (1) stress-relaxation tests at -40, -30, -20, and 20°C and at about 6 axial extension ratios between about 1.25 and 2.50; and (2) tests at 5 to 8 constant extension rates at 25, 35, 50, 70, and 90°C. In addition, data in uniaxial tension were obtained at 10 extension rates at the five temperatures between 25 and 90°C.

The cylindrical specimens for biaxial tests, prepared at the Air Force Materials Laboratory, have an inside diameter of 1.50 inches, a wall thickness of about 0.048 inch, and a 6-inch gage section. To obtain a precise value for the extension ratio (λ_1) in the axial direction,

seven fiducial marks were inscribed around the circumference of a specimen at approximately 1-inch intervals along the gage section. This was accomplished by placing a specimen on a mandrel which was then turned slowly on a lathe while lines were drawn with a fine ballpoint pen. In addition, one or more vertical lines were drawn lengthwise along the gage section to aid in vertical alignment of a specimen at the beginning of a test and to facilitate obtaining precise cathetometer readings of the fiducial lines.

Table I

DATA WHICH SHOW COMPLETENESS OF RECOVERY OF CYLINDRICAL SPECIMEN AFTER EACH TEST IN A SERIES

Number of Stretches	Length (cm) Between Outer Bench Marks After Recovery Period
0	15.210
1	15.545
2	15.570
3	15.580
4	15.595
5	15.570
6	15.570
7	15.590
8	15.565
9	15.590
10	15.585
11	15.600
12	15.585
13	15.610
14	15.590

All stress-relaxation tests were made using only two specimens (special tests were made on other specimens). After a test, the specimen was allowed to recover at room temperature for no less than one day before it was used in another test. Subsequent to each recovery period, it was found that the specimen had regained quite closely its original length. Data which show that the recovery was essentially complete are in Table I. This table shows that, after the specimen had recovered from the first stretch, the distance between the two extreme bench marks had increased 0.235 cm, or 1.5%. After the second extension, the length was about 0.035 cm greater than prior to the second stretch; an increase of about 0.23%. However, following each subsequent extension, the length was nearly the same, remaining between 15.57 and 15.61 cm. The stress-relaxation data did not appear to depend on the particular specimen tested or on the number of times that a specimen had been stretched.

Prior to making a test, a spare specimen was mounted in the apparatus and stretched to approximately the extension at which relaxation data were desired. Gas pressure was admitted to the specimen and the position of the sensing probe, used to control the pressure, was adjusted until the outside diameter of the specimen was 1.596 inches. Although the diameter was carefully determined with precision calipers, the measurement was accurate only to about 0.01 inch, or possibly slightly more. Greater accuracy was not possible because the specimen deformed somewhat when contacted with the calipers. In carrying out many of the tests, the outside diameter was inadvertently set at about 1.54 inches. Because the stress-relaxation data, especially at relatively small extensions, are quite sensitive to the precise diameter of the specimen during a test, data from tests made at a diameter of 1.54 inches were corrected to a diameter of about 1.60 inches. The method for making this correction is discussed in Section II-D.

After the sensing probe had been positioned, the spare specimen was removed from the apparatus. Next, a test specimen was mounted and clamped on the lower end piece and allowed to attain thermal equilibrium in the temperature-controlled cabinet (containing a multi-pane window) on the Instron tester. After the positions of the seven fiducial marks were read with a cathetometer, the upper end of the specimen was clamped and the Instron crosshead was lowered at 20 inches per minute (the maximum possible rate) until the desired extension ratio (λ_1) was reached. During this extension, nitrogen gas was admitted into the specimen; the rate was controlled by the sensing probe so that a fixed outside diameter was maintained. While the specimen was maintained at a fixed elongation and diameter, the axial load and the gas pressure were recorded during a period of two to three hours. In addition, the positions of the fiducial marks on the stretched specimen were read; these readings along with the initial values were used to derive λ_1.

The method for deriving λ_1 from the cathetometer readings of the fiducial lines on the stretched and unstretched specimen is possibly novel and thus will be described in some detail. Suppose we designate

the reading for each fiducial mark on the stretched specimen by $(R_s)_i$ and on the unstretched specimen by $(R_u)_i$, where i = 1,2,3 . . . 7 (we are here considering seven fiducial marks). To illustrate the method, suppose we have two other readings, $(R_s)_o$ and $(R_u)_o$, where for the moment these may be considered to be readings for another mark on the specimen. We can now write:

$$\frac{(R_s)_i - (R_s)_o}{(R_u)_i - (R_u)_o} = \lambda_1 \tag{12}$$

This equation, which is valid for any value of i, can be rewritten to give:

$$(R_s)_i = \lambda_1 (R_u)_i + (R_s)_o - \lambda_1 (R_u)_o \tag{13a}$$

$$= \lambda_1 (R_u)_i + K \tag{13b}$$

where K is a constant which equals $(R_s)_o - \lambda_1 (R_u)_o$. Equation (13) shows that a plot of $(R_s)_i$ vs $(R_u)_i$ will yield a straight line whose slope is λ_1, provided the extension ratio is the same at all points on the gage section between the first and the seventh fiducial marks. Equation (13) also indicates that $(R_s)_o$ and $(R_u)_o$ need not be known; in fact, these quantities were introduced only to show clearly that the slope of a plot of $(R_s)_i$ vs $(R_u)_i$ equals λ_1.

The above method was used to obtain highly accurate values of λ_1; in general, the accuracy appeared to be within $\pm$ 0.5%, and commonly better. Table II provides illustrative data. Both sets of data are represented quite precisely by the equations beneath the table. (In the table, the subscript i has been omitted from the symbols R_s and R_u.) Data in the table show that the differences between the observed values of R_s and those computed from the equation are quite small, especially in the case of $\lambda_1 = 1.47$. For $\lambda_1 = 2.26$, the differences are somewhat greater and the tabulated values show that the experimental values of R_s lie along a shallow curve, instead of a straight line. Although this

Table II

COMPARISON OF CATHETOMETER READINGS WITH VALUES CALCULATED FROM A LINEAR EQUATION

Fiducial Mark	$\lambda_1 = 1.47$				$\lambda_1 = 2.26$			
	R_u (cm)	R_s (cm)			R_u (cm)	R_s (cm)		
		Obs.	Calc.[a]	Diff.		Obs.	Calc.[b]	Diff.
1	85.050	77.600	77.57	-0.03	82.420	62.325	61.86	-0.365
2	87.635	81.380	81.37	-0.01	85.165	68.175	68.07	-0.105
3	90.210	85.175	85.16	-0.015	87.740	73.950	73.69	-0.26
4	92.785	88.985	88.95	-0.035	90.355	76.760	79.80	0.04
5	95.275	92.655	92.61	-0.045	92.955	85.740	85.68	-0.06
6	97.870	96.465	96.43	-0.035	95.660	92.105	91.79	-0.315
7	100.400	100.135	100.14	0.005	98.270	97.830	97.69	-0.14

a. Computed from the equation: $R_s = 1.4707\ R_u - 47.51$.

b. Computed from the equation: $R_s = 2.2600\ R_u - 124.40$.

behavior suggests that the extension is slightly nonuniform along the gage section, the variation is indeed quite small.

This new method of determining the extension ratio appears to have the following advantages over that previously used:[4] (1) nonuniform strain along the gage section can be readily detected; and (2) the fiducial marks need not be evenly spaced--a necessary condition for application of the previous method. It is planned to apply the new procedure to obtain λ_1 from photographs made of the fiducial marks during tests at constant extension rates.

After the first relaxation test had been performed and a value of λ_1 had been obtained, an effective gage length L_e = (crosshead travel)/(λ_1 - 1) was calculated. Then it was possible to calculate the crosshead travel required to give approximately the extension ratio desired in subsequent tests. Because a specimen was remounted on the end pieces

before each test, the actual value of L_e varied slightly among tests. However, for each test the specimen was mounted and clamped in as nearly identical a fashion as possible, and the variation in L_e among tests was accordingly small. Essentially all values obtained for L_e lay between 6.40 and 6.80 inches; the average of numerous determinations was about 6.65 inches. For the earlier tests[4] made at constant extension rates, crosshead displacement was converted into $\lambda_1 - 1$ by using an effective gage length of 6.40 inches. (This value is the average of those obtained by photographing fiducial marks during each test.) Since the specimens for these tests may have been mounted slightly differently than for the relaxation tests, the agreement between the L_e values from the two methods is quite good. It is concluded that L_e = 6.40 inches was probably the best single value to use in reducing the constant extension rate data.

Biaxial relaxation tests were made at six extension ratios between about 1.25 and 2.50 at each test temperature except -40°C. At this low temperature, data could not be obtained at λ_1 greater than 2.0 because of an instability in the cylindrical specimen. The instability consisted of a ballooning in a gage section. The reason for this instability is discussed briefly in Section IV-A.

Each test gave the following raw data: the force in the axial direction sensed by the load cell of the Instron tester; the gas pressure inside the specimen; and the extension ratio λ_1 at which the relaxation data were obtained. From these quantities along with the dimensions of a specimen at 25°C, $\bar{\sigma}_1$ and $\bar{\sigma}_2$ were computed, where $\bar{\sigma}_1$ is the average stress (based on the cross-sectional area of the deformed specimen at the test temperature) in the axial direction and $\bar{\sigma}_2$ is the circumferential stress evaluated on the outside surface of the specimen.* The equations for these computations are included in the discussion

*Actually, the circumferential stress ($\bar{\sigma}_2$) based on deformed cross-sectional area equals the engineering stress σ_2 since the area over which the hoop tension acts is independent of the magnitude of λ_1, provided $\lambda_2 = 1.0$.

previously given.[4] In making the calculations, it was assumed that at 25°C the inside diameter of each specimen is 1.50 inches and that the wall thickness is 0.048 inch; the change in these dimensions with temperature was accounted for by using the coefficient of thermal expansion for SBR-IV.

As discussed in Ref. 4, $\bar{\sigma}_1$ varies slightly across the wall of the specimen. However, $\bar{\sigma}_1$ on the outside surface differs from the average value by 1 to 3%, depending on λ_1 and the properties of the material.

Calculations were also made of the values of $\bar{\sigma}_1$ and $\bar{\sigma}_2$ which develop during the extension of a specimen to the particular value of λ_1 at which relaxation measurements were made. For these calculations, λ_1 as a function of time was derived from crosshead travel and the effective gage length was derived, as mentioned above, from cathetometer readings on the fiducial marks on the specimen.

The experimental aspects of the tests at a series of constant extension rates have already been described.[4] The data were reduced in a manner similar to that for reducing the stress-relaxation data, except that for each test λ_1 was obtained from crosshead displacement using an L_e of 6.40 inches. The major difference in the calculation is that values of $\bar{\sigma}_1$ and $\bar{\sigma}_2$ were first obtained at a large number of values of λ_1 and then by interpolation at a series of fixed values of λ_1. Thus, plots could be made of log $\bar{\sigma}_1$ vs log t and log $\bar{\sigma}_2$ vs t, where points along single curves correspond to a constant value of λ_1 and where the time t equals $(\lambda_1 - 1)/\dot{\lambda}_1$; $\dot{\lambda}_1$ is the extension rate which equals the crosshead speed divided by L_e.

C. Uniaxial Tensile Data

Constant extension rate tests in uniaxial tension were made on rings cut from cylindrical specimens of SBR-IV. Tests were made at crosshead speeds between 0.02 and 20 inches per minute at 25, 35, 50, 70, and 90°C. Other aspects of the test procedure have been discussed previously and the rupture data have been presented.[4]

The data were evaluated in the usual manner[1-4] by first preparing the plots of log σ vs log t, where σ along each line corresponds to a fixed value of λ; such plots gave a series of parallel straight lines at each temperature. As shown in Table III, the lines from all plots had negative slopes, indicating that equilibrium response was not achieved even at the highest test temperature.

Table III

MOONEY-RIVLIN PARAMETERS AND MODULUS VALUES FROM ISOCHRONAL DATA ON SBR-IV IN UNIAXIAL TENSION

Temp. ($^{\circ}$C)	M[(a)]	$2C_1$	$2C_2$	F(1)[(b)] (psi)
25	0.015	34.4	60.1	257
35	0.012	36.8	59.2	260
50	0.018	38.5	57.0	258
70	0.016	38.7	57.8	262
90	0.011	36.0(?)	59.0	267

(a) $M = -(d \log \sigma / d \log t)$, the slope of plots of log σ vs log t.

(b) F(1) = one-minute modulus from plot of $\lambda\sigma$ vs $(\lambda-1)$.

One-minute isochronal stress-strain data were obtained from the plots of log σ vs log t, and these were used to derive the temperature-dependent Mooney-Rivlin parameters C_1 and C_2. Values of $2C_1$ and $2C_2$ at each temperature were obtained from the intercept and slope, respectively, of plots of $\sigma(1)/(\lambda-\lambda^{-2})$ vs $1/\lambda$, where $\sigma(1)$ is the 1-minute stress value. Both $2C_1$ and $2C_2$ are slightly temperature-dependent, as shown in Table III; $2C_1$ increases with temperature whereas $2C_2$ decreases. The data become increasingly less accurate as the temperature is increased because specimens ruptured at progressively lower elongations and thus only limited data were available at elevated temperatures for the Mooney-Rivlin plots.

One-minute isochronal values of the stress were also used to determine the one-minute modulus F(1) from the slopes of plots of $\lambda\sigma(1)$ vs λ-1. These plots were linear at extensions below about 30%; above 30%, the plots curved downward slightly. As shown in Table III, F(1) tends to increase somewhat with temperature.

D. Biaxial Tensile Data

1. Time Dependence of Data

As already mentioned, tests were made at 25, 35, 50, 70, and 90°C at 5 to 8 crosshead speeds between 0.02 and 20 inches per minute. Data at 35°C are shown in Fig. 2 by plots of log $\bar{\sigma}_1$ vs log t and log $\bar{\sigma}_2$ vs log t at values of λ_1 between 1.1 and 2.4. Results at other temperatures were similar. Stress-relaxation tests were made at 20, -20, -30, and -40°C at extension ratios of about 1.25, 1.50, 1.75, 2.00, 2.25, and 2.50. (At -40°C, data could not be obtained at λ_1 values of 2.25 and 2.50 because the specimen ballooned in the gage section.) For illustrative purposes, data at -30°C are shown in Fig. 3.

In all instances, data like those in Figs. 2 and 3 could be represented by parallel curves; data from the constant extension rate tests could be represented by straight lines whereas curves were required to fit the relaxation data. Within the experimental uncertainty, $d \log \bar{\sigma}_1 / d \log t \equiv -M_1$ was found to equal $d \log \bar{\sigma}_2 / d \log t \equiv -M_2$, as shown by the results in Table IV. (From the relaxation data, M_1 and M_2 were evaluated at a time of 10 minutes.) Again within the experimental uncertainty, M_1 from uniaxial tests at constant rates of extension were found (Table IV) to equal those from the biaxial tests. However, the relaxation rate was quite small (2 to 4% per decade of time) and thus no firm conclusion can be drawn from this observation. Even at low temperatures, at which uniaxial tests were not made, the relaxation rate was relatively small, being about 9 and 12% per decade of time at -30 and -40°C, respectively.

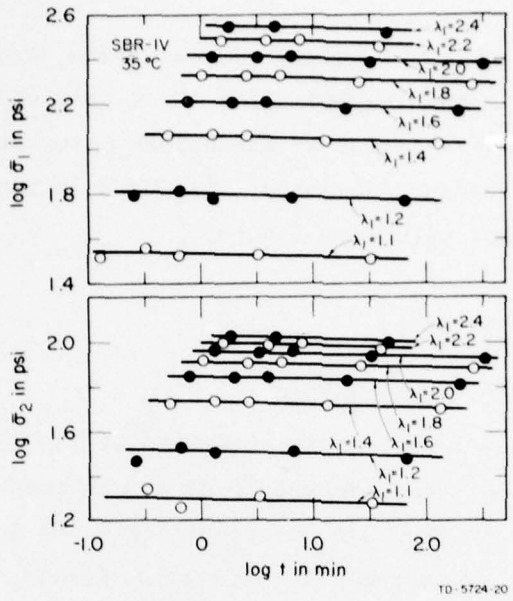

FIG. 2 PLOTS OF LOG $\bar{\sigma}_1$ AND LOG $\bar{\sigma}_2$ vs LOG t.
Data from biaxial tests at constant extension rates at 35 °C on SBR-IV.

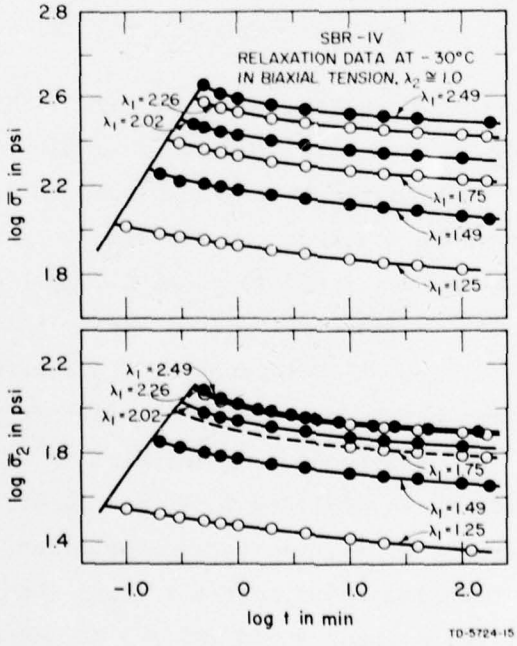

FIG. 3 PLOTS OF LOG $\bar{\sigma}_1$ AND LOG $\bar{\sigma}_2$ vs LOG t.
Data from biaxial stress-relaxation tests at -30 °C on SBR-IV.

Table IV

RELAXATION RATE OF SBR-IV IN BIAXIAL AND UNIAXIAL TENSION AT DIFFERENT TEMPERATURES

Temp. °C	Biaxial Tests				Uniaxial Tests at Constant $\dot{\lambda}$,
	Constant λ		Constant $\dot{\lambda}$		
	M_1(a)	M_2(b)	M_1	M_2	M_1
-40	0.05	0.050			
-30	0.040	0.040			
-20	0.025	0.025			
20	0.015	0.015			
25			0.010	0.015	0.015
35			0.015	0.015	0.012
50			0.010	0.010	0.018
70			0.010	0.015	0.016
90			0.010	0.010	0.011

(a) $M_1 = -\dfrac{d \log \bar{\sigma}_1}{d \log t}$

(b) $M_2 = -\dfrac{d \log \bar{\sigma}_2}{d \log t}$

2. Isochronal Data

One-minute isochronal data were read from the plots of log $\bar{\sigma}_1$ and log $\bar{\sigma}_2$ vs log t, illustrated by Fig. 2, and used to prepare a plot of $\bar{\sigma}_1/\bar{\sigma}_2$ vs $\lambda_1 - 1$ (not shown). Similarly, 10-minute isochronal data were read from the plots representing the stress-relaxation data. When these were included on the plot of $\bar{\sigma}_1/\bar{\sigma}_2$ vs $\lambda_1 - 1$, it was found that data from the relaxation tests lay somewhat above those from the constant extension rate tests. Also, at small extensions, $\bar{\sigma}_1/\bar{\sigma}_2$ from the relaxation tests increased with decreasing $\lambda_1 - 1$ instead of continuing to decrease toward a value of 2.0 at $\lambda_1 - 1$, as predicted by Eq. (9). The lack of agreement between $\bar{\sigma}_1/\bar{\sigma}_2$ from relaxation and constant rate tests was attributed to the fact that λ_2 was slightly less than unity during the relaxation tests,

as mentioned in Section II-B. In fact, special tests verified that $\bar{\sigma}_1/\bar{\sigma}_2$ is very sensitive to the precise value of λ_2, especially at small extensions.

The sensitivity of $\bar{\sigma}_1$ and $\bar{\sigma}_2$ to the precise value of λ_2 at which a test is made can be seen by employing Eqs. (1) and (2) to obtain relations between $(\bar{\sigma}_1)_c$ and $(\bar{\sigma}_1)_o$ and between $(\bar{\sigma}_2)_c$ and $(\bar{\sigma}_2)_o$, where $(\bar{\sigma}_1)_o$ and $(\bar{\sigma}_2)_o$ are values at a λ_2 different from unity and $(\bar{\sigma}_1)_c$ and $(\bar{\sigma}_2)_c$ are values at $\lambda_2 = 1$. The resulting equations (obtained by recalling that $\bar{\sigma}_3 = 0$ and $\lambda_3 = \lambda_1^{-1}$ on the outside of the specimen) are:

$$\frac{(\bar{\sigma}_1)_c}{(\bar{\sigma}_1)_o} = \frac{(\lambda_1^2 - \lambda_1^{-2})(1 + \alpha)}{(\lambda_1^2 - \lambda_2^{-2}\lambda_1^{-2})(1 + \lambda_2^2\alpha)} \tag{14}$$

$$\frac{(\bar{\sigma}_2)_c}{(\bar{\sigma}_2)_o} = \frac{1 - \lambda_1^{-2}}{(\lambda_2^2 - \lambda_2^2\lambda_1^{-2})} \tag{15}$$

where $\alpha \equiv W_2/W_1$

Although Eqs. (14) and (15) can be readily solved, provided α is known, we shall now consider that λ_2 is relatively close to unity and only examine two limiting cases.

Case 1: $\lambda_1 \gg 1$. In this instance, Eqs. (14) and (15) reduce to:

$$\frac{(\bar{\sigma}_1)_c}{(\bar{\sigma}_1)_o} = \frac{(1 + \alpha)}{(1 + \lambda_2^2\alpha)} \tag{16}$$

$$\frac{(\bar{\sigma}_2)_c}{(\bar{\sigma}_2)_o} = \lambda_2^{-2} \tag{17}$$

If $\lambda_2 = 0.97$ and $\alpha = 0.3$, then we find that $(\bar{\sigma}_1)_c/(\bar{\sigma}_1)_o = 1.01$ and $(\bar{\sigma}_2)_c/(\bar{\sigma}_2)_o = 1.06$; this illustrates that at high extensions $\bar{\sigma}_1$ is relatively insensitive to λ_2 whereas $\bar{\sigma}_2$ is still quite dependent on λ_2.

Case 2: $\epsilon_2 \ll \epsilon_1 \lesssim 0.2$, where $\epsilon_2 = \lambda_2 - 1$ and $\epsilon_1 = \lambda_1 - 1$. Under these conditions, Eqs. (14) and (15) give:

$$\frac{(\bar{\sigma}_1)_c}{(\bar{\sigma}_2)_o} \simeq \frac{1}{(1 + \frac{\epsilon_2}{2\epsilon_1} - \epsilon_2)(1 + \frac{2\epsilon_2\alpha}{1+\alpha})} \tag{18}$$

$$\frac{(\bar{\sigma}_2)_c}{(\bar{\sigma}_2)_o} = \frac{1}{1 + \frac{2\epsilon_2}{\epsilon_1}} \tag{19}$$

Again let us suppose that $\epsilon_2 = -0.03$ ($\lambda_2 = 0.97$) and $\alpha = 0.3$ and then consider the situation when $\epsilon_1 = 0.10$ ($\lambda_1 = 1.10$). Under these conditions, $(\bar{\sigma}_1)_c/(\bar{\sigma}_1)_o = 1.15$ and $(\bar{\sigma}_2)_c/(\bar{\sigma}_2)_o = 2.5$. This example illustrates that, at small values of λ_1, $\bar{\sigma}_2$ is strongly dependent on λ_2 but that $\bar{\sigma}_1$ is only moderately dependent on λ_2.

In carrying out experiments on the cylindrical specimens, it is quite likely, even when extreme precautions are taken, that λ_2 will lie somewhere between 0.995 and 1.005; it is not unlikely in certain instances that the uncertainty in λ_2 will be somewhat larger, e.g., $\pm$ 1%. However, if $\lambda_2 = 0.995$ ($\epsilon_2 = -0.005$), then $(\bar{\sigma}_2)_c/(\bar{\sigma}_2)_o = 1.11$ at $\lambda_1 = 1.10$. This result illustrates the great difficulty in obtaining highly accurate values of $\bar{\sigma}_2$ at small values of λ_1.

In conducting the relaxation tests, the outside diameter of the cylindrical specimens was inadvertently regulated at values close to 1.54 inches instead of at the desired value 1.596 inches. During any single test, however, the diameter undoubtedly varied by less than 0.01 inch. Thus Eqs. (14) and (15) were employed to correct the observed values of $\bar{\sigma}_1$ and $\bar{\sigma}_2$ to those that correspond to $\lambda_2 = 1.0$.

To make the correction, values of W_1 and W_2, and thus of α, were derived from the constant extension rate data. (It is believed that λ_2 remained quite close to unity during these tests.) The values of α, which depend on λ_1 but which need not be accurately known, were used to

correct the observed 10-minute isochronal values of $\bar{\sigma}_1$ and $\bar{\sigma}_2$, according to Eqs. (14) and (15); the calculation was made for several values of λ_2. Then, the ratio $\bar{\sigma}_1/\bar{\sigma}_2$, from corrected data, was compared with data from the constant extension rate tests. This comparison showed that the best value to assume for λ_2 was 0.975; this value was used in correcting the data.

3. Determination of Strain Functions

Ten-minute isochronal data, corrected to $\lambda_2 = 1.0$, were used along with 1-minute isochronal data from the constant extension rate tests to prepare plots of log $\bar{\sigma}_1$ and log $\bar{\sigma}_2$ vs log $(\lambda_1 - 1)$. Plots representing the relaxation data are shown in Fig. 4.

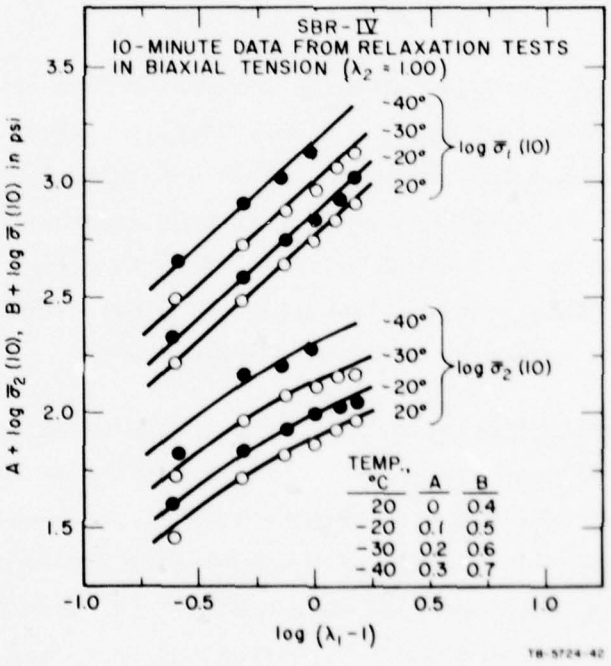

FIG. 4 TEN-MINUTE ISOCHRONAL STRESS-STRAIN DATA FROM BIAXIAL STRESS-RELAXATION TESTS AT TEMPERATURES BETWEEN 20 AND -40°C

As discussed in Section II-B and illustrated in Fig. 1, an accurate value of the small deformation shear modulus cannot be obtained from curves like those shown in Fig. 4. Thus, values of F(1)/3, which equals the shear modulus, from the uniaxial tensile data (Table III) were used in reducing the biaxial data from the constant extension rate tests. The data are shown in Fig. 5 by plots of log $3\bar{\sigma}_1(1)/F(1)$ and log $3\bar{\sigma}_2(1)/F(1)$ vs log $(\lambda_1 - 1)$. The dotted lines, which merge with the solid curves at small extensions, have a unit slope, are separated by 0.30 logarithmic unit (a factor of two), and at log $(\lambda_1 - 1) = 0$ they give $3\bar{\sigma}_1(1)/F(1) = 4.0$ and $3\bar{\sigma}_2(1)/F(1) = 2.0$. In other words, they represent

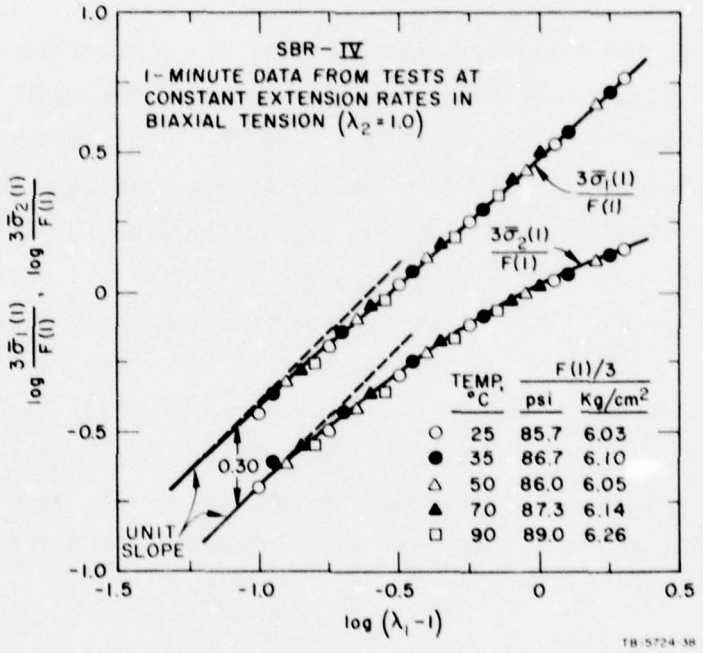

FIG. 5 PLOTS OF LOG $3\bar{\sigma}_1(1)/F(1)$ AND LOG $3\bar{\sigma}_2(1)/F(1)$ vs LOG $(\lambda_1 - 1)$ PROVIDED BY 1-MINUTE ISOCHRONAL DATA FROM BIAXIAL TESTS AT CONSTANT EXTENSION RATES AT TEMPERATURES BETWEEN 25 AND 90°C. The quantity F(1) is the 1-minute constant extension rate modulus from uniaxial tensile tests.

the equations $\bar{\sigma}_1 = 4G(\lambda_1 - 1)$ and $\bar{\sigma}_2 = 2G(\lambda_1 - 1)$. Because these equations provided by classical elasticity must hold in the limit of zero strain, the solid curves (representing experimental data) must approach the dotted lines at small strains. Figure 5 shows that the experimental data conform to this expectation. In addition, the figure shows that data at the five temperatures between 25 and 90°C superpose to define quite precisely the individual curves. It perhaps should be explicitly pointed out that data at times other than 1 minute would yield curves identical to those in Fig. 5; this follows because the relaxation rate, as given by d log σ/d log t, in uniaxial tension is the same as for the $\bar{\sigma}_1$ and $\bar{\sigma}_2$ data from the biaxial tests and because the relaxation rate in each instance is independent of the magnitude of λ_1.

To reduce the stress-relaxation data, the plots (Fig. 4) of log $\bar{\sigma}_1(10)$ vs log $(\lambda_1 - 1)$ were shifted along the ordinate to effect superposition; similarly, the log $\bar{\sigma}_2(10)$ vs log $(\lambda_1 - 1)$ curves were superposed. The shift distances give relative values of the 10-minute shear modulus; the relative values from superposing the $\bar{\sigma}_1(10)$ data were sensibly identical with those from superposing the $\bar{\sigma}_2(10)$ data. To obtain the shear modulus at 20°C, the curves representing isochronal data at 20°C were shifted vertically to superpose with those in Fig. 5. (Again, the superposition of the $\bar{\sigma}_1$ and $\bar{\sigma}_2$ data gave the same shift distances.) From the modulus at 25°C [specifically, from F(1)/3] and the shift distance, the 10-minute relaxation shear modulus, G(10), was obtained* at 20°C; values of G(10) at lower temperatures were then derived from the relative values of G(10).

*Because F(1)/3 is the shear modulus from constant extension rate tests, it should have been converted, strictly speaking, into G(1), the 1-minute stress-relaxation modulus, before deriving G(10) at 20°C. The conversion equation[14] is G(1) = [F(1)/3][1 + d log F(1)/d log t]; since d log F(1)/d log t is about -0.015, G(1) and F(1)/3 differ by only 1.5%, a small difference which can be neglected.

Plots were next prepared of log $\bar{\sigma}_1(10)/G(10)$ and log $\bar{\sigma}_2(10)/G(10)$ vs log $(\lambda_1 - 1)$ and these are shown in Fig. 6. The solid curves, which have been drawn to be identical with those in Fig. 5, represent the stress-relaxation data between 20 and -40°C quite precisely. The tabulations of modulus values in Figs. 5 and 6 show that G(10) at 20°C is 74.6 psi and that F(1)/3 at 25°C is 85.7 psi. This difference undoubtedly arises because the specimens for the relaxation tests were prepared at a later date than those from the constant extension rate tests and probably were not cured to the same extent.

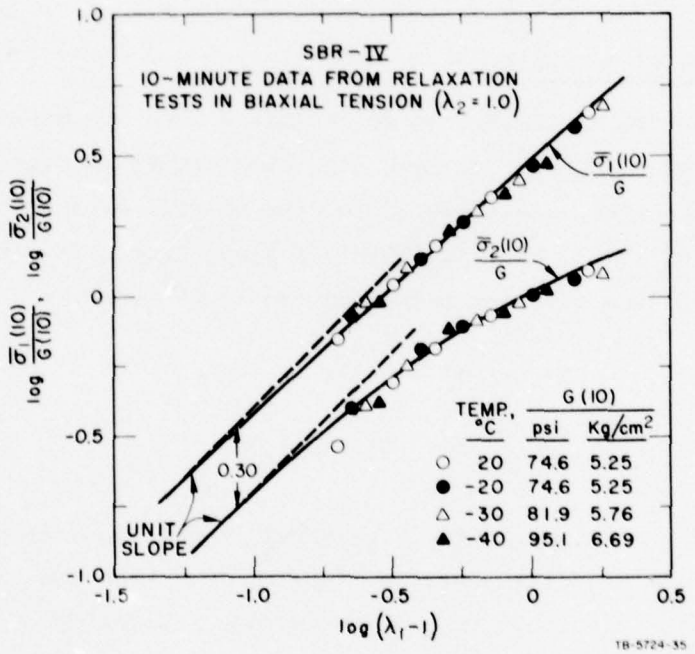

FIG. 6 PLOTS OF LOG $\bar{\sigma}_1(10)/G(10)$ AND LOG $\bar{\sigma}_2(10)/G(10)$ vs LOG $(\lambda_1 - 1)$ PROVIDED BY 10-MINUTE ISOCHRONAL DATA FROM BIAXIAL STRESS-RELAXATION TESTS AT TEMPERATURES BETWEEN 20 AND -40°C. The quantity G(10) is the 10-minute stress-relaxation modulus in shear. The curves are identical to those in Fig. 5.

Because all biaxial data between -40 and 90°C can be represented by two curves (those in Fig. 5 are identical with those in Fig. 6), it follows that the data are given by:

$$\bar{\sigma}_1(\lambda_1, t, T) = 4G(t,T)\Gamma_1(\lambda_1) \tag{20}$$

$$\bar{\sigma}_2(\lambda_1, t, T) = 2G(t,T)\Gamma_2(\lambda_1) \tag{21}$$

where $G(t,T)$ is the shear modulus at time t and temperature T, and $\Gamma_1(\lambda_1)$ and $\Gamma_2(\lambda_1)$ are different functions of λ_1; both of these strain functions reduce to $(\lambda_1 - 1)$ in the limit of zero strain.

E. Evaluation of W_1 and W_2

The quantities W_1 and W_2 can be evaluated from the biaxial data in Figs. 5 and 6 by using Eqs. (3) and (4), upon recalling that $\bar{\sigma}_3 = 0$, $\lambda_2 = 1.0$, and $\lambda_3 = \lambda_1^{-1}$. As shown above, the biaxial data are represented by Eqs. (20) and (21). Upon substituting these expressions for $\bar{\sigma}_1$ and $\bar{\sigma}_2$ into Eqs. (3) and (4), the following equations* result:

$$2W_1(\lambda_1, t) = G(t)\chi_1(\lambda_1) \tag{22}$$

$$2W_2(\lambda_1, t) = G(t)\chi_2(\lambda_1) \tag{23}$$

where $W_1(\lambda_1, t)$ and $W_2(\lambda_1, t)$ are, in general, functions** of λ_1 and t; $\chi_1(\lambda_1)$ and $\chi_2(\lambda_1)$ are different functions of λ_1. From the discussion in Section II-A, it follows that W_1 and W_2 are strain-independent at sufficiently small strains and thus $2[W_1(t) + W_2(t)] = G(t)$ under such conditions.

---

*It is here assumed that time-temperature superposition is valid and thus t in Eqs. (22) and (23) should be considered to be t/a_T, where a_T is the time-temperature shift factor.

**More precisely, W_1 and W_2 are functions of I_1 and I_2 as well as of time. In the present case, however, $I_1 = I_2 = \lambda_1^2 + \lambda_1^{-2} + 1$.

To evaluate $2W_1(\lambda_1,t)/G(t)$ and $2W_2(\lambda_1,t)/G(t)$ (these quantities equal the strain functions $\chi_1(\lambda_1)$ and $\chi_2(\lambda_1)$, respectively), Eqs. (3) and (4) can be written as follows:

$$\frac{1}{G}\left(\frac{\lambda_1^2\bar{\sigma}_1}{\lambda_1^2 - \lambda_1^{-2}} - \frac{\bar{\sigma}_2}{1 - \lambda_1^{-2}}\right) = \frac{2W_1}{G}(\lambda_1^2 - 1) \qquad (24)$$

$$\frac{1}{G}\left(\frac{\bar{\sigma}_2}{1 - \lambda_1^{-2}} - \frac{\bar{\sigma}_1}{\lambda_1^2 - \lambda_1^{-2}}\right) = \frac{2W_2}{G}(\lambda_1^2 - 1) \qquad (25)$$

where for simplicity the dependence of G on t, and of W_1 and W_2 on λ_1 and t is not specifically indicated.

The left side of Eq. (24) and also of Eq. (25) was computed from data read from the curves in Fig. 6 (identical to those in Fig. 5) and these quantities are plotted against λ_1^2-1 in Figs. 7 and 8. Figure 7 shows that $2W_1/G = 0.625$ for values of λ_1 up to about 2.0 ($I_2 = I_1 = 5.25$); thereafter it decreases somewhat with increasing λ_1. Figure 8 shows that $2W_2/G$ decreases continually with increasing λ_1. The dotted line was drawn having a slope of 0.357; this slope, which equals the initial value of $2W_2/G$, was selected to satisfy the relation $2W_1/G + 2W_2/G = 1$, where $2W_1/G = 0.625$, as shown in Fig. 7.

Figure 9 shows $2W_1/G$, $2W_2/G$, and W_2/W_1 plotted against I_1-3 = I_2-3. The values of $2W_1/G$ and $2W_2/G$ were obtained by reading ordinate values from the curves in Figs. 7 and 8 and dividing these by the corresponding values of λ_1^2-1. The resulting data along with W_2/W_1 are tabulated in Table V. The dependence of $2W_2/G$ on I_1-3 = I_2-3 is qualitatively similar to the dependence of $2W_2$ on I_2-3 found by Rivlin and Saunders[6] for a natural rubber vulcanizate. (From their extensive study, they suggested that W_2 is a function only of I_2 and that W_1 is a constant.) In the present study, however, data were obtained only in pure shear for which $I_1 = I_2$, and thus it is not possible to state whether $2W_2/G$ is independent of I_1 and likewise whether $2W_1/G$ is independent of I_2. The data do indicate, however, that $2W_1/G$ decreases at values of $I_1 = I_2$ greater than about 5.3.

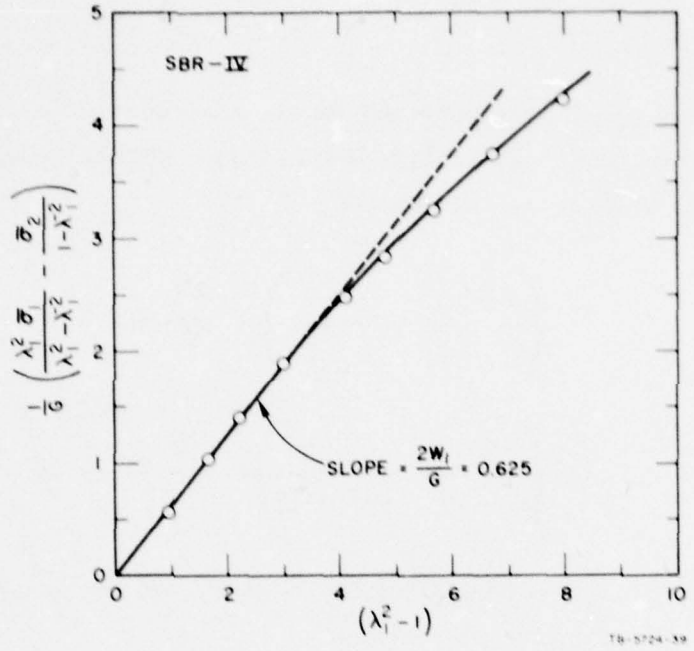

FIG. 7 DATA FROM FIGS. 5 AND 6 PLOTTED TO EVALUATE $2W_1/G$ ACCORDING TO EQ. (24)

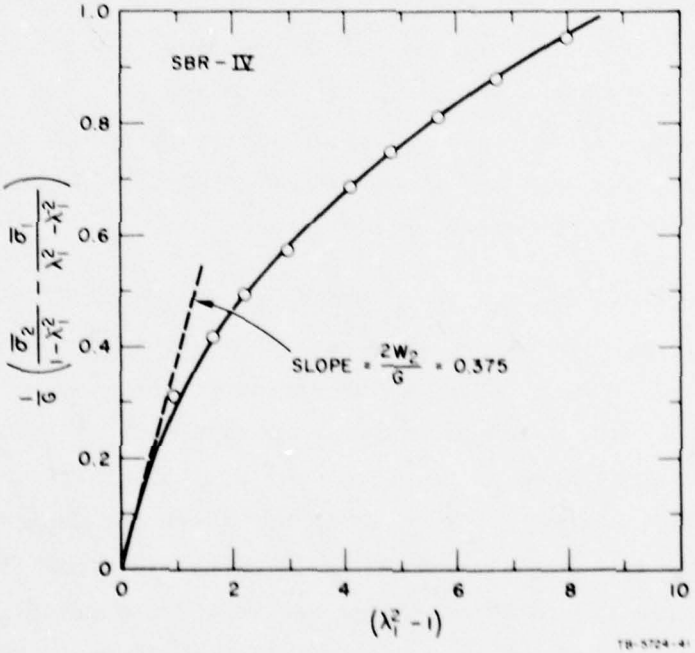

FIG. 8 DATA FROM FIGS. 5 AND 6 PLOTTED TO EVALUATE $2W_2/G$ ACCORDING TO EQ. (25)

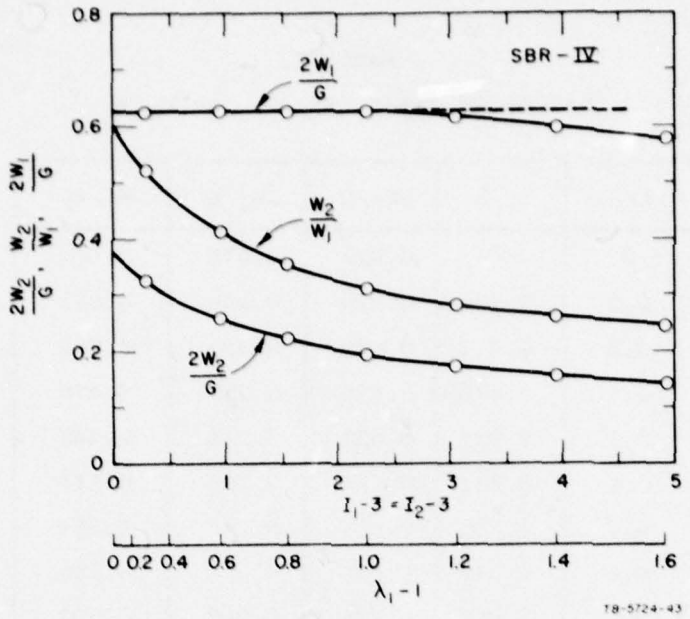

FIG. 9 PLOTS OF $2W_2/G$, W_2/W_1, AND $2W_1/G$ vs $I_1-3 = I_2-3$
(Quantities evaluated from curves in Figs. 7 and 8.)

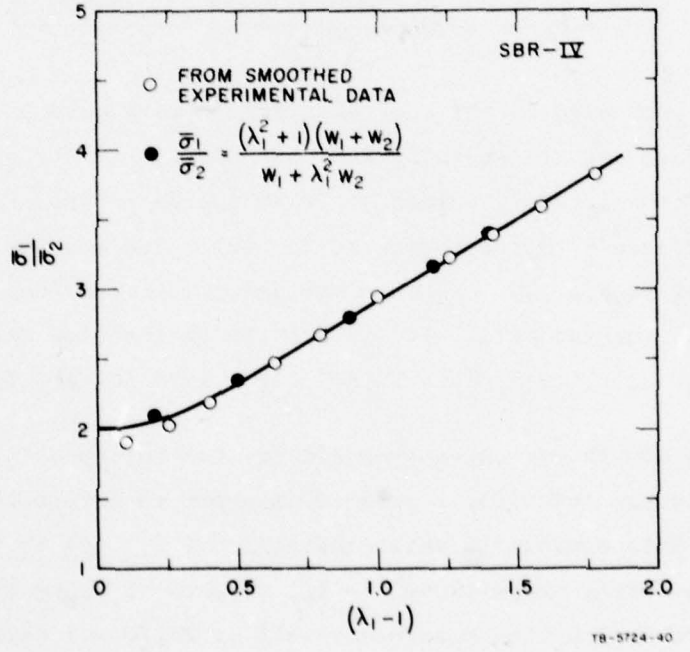

FIG. 10 PLOT OF $\bar{\sigma}_1/\bar{\sigma}_2$ vs λ_1-1. Open circles represent data from curves in Figs. 5 and 6 and solid circles represent those obtained by inserting values of $2W_1/G$ and $2W_2/G$ in Eq. (9).

Table V

VALUES OF $2W_1/G$, $2W_2/G$, AND W_2/W_1

$\lambda_1 - 1$	$I_1 - 3$	$2W_1/G$	$2W_2/G$	W_2/W_1
0	0	0.625	0.375	0.600
0.2	0.134	0.625	0.359	0.574
0.3	0.282	0.625	0.326	0.522
0.4	0.470	0.625	0.297	0.475
0.5	0.694	0.625	0.278	0.445
0.6	0.951	0.625	0.258	0.413
0.7	1.236	0.625	0.240	0.384
0.8	1.549	0.625	0.222	0.355
0.9	1.887	0.625	0.207	0.331
1.0	2.250	0.625	0.193	0.310
1.2	3.047	0.615	0.173	0.281
1.4	3.934	0.597	0.156	0.262
1.6	4.908	0.578	0.142	0.245

Data represented by the curves in Fig. 6 were used to obtain $\bar{\sigma}_1/\bar{\sigma}_2$ and selected values are shown by the open circles in Fig. 10. To check for internal consistency, values of $2W_1/G$ and $2W_2/G$ from Fig. 9 were used to calculate $\bar{\sigma}_1/\bar{\sigma}_2$ according to Eq. (9). The results, shown by solid circles in Fig. 10, are in close agreement with those from the smoothed experimental data. It is of interest that the data are represented by the equation $\bar{\sigma}_1/\bar{\sigma}_2 = 1.18(\lambda_1 - 1) + 1.74$ for $(\lambda_1 - 1) > 0.5$.

As Gent and Thomas[7] have proposed Eq. (6) to represent approximately the strain energy function, it was of interest to determine how closely the present data conform to this equation. If Eq. (6) is valid, $2W_2$ should be inversely proportional to I_2. Figure 11 shows that the present data are represented reasonably well by $2W_2/G = 1.04/I_2$. Although this equation is possibly invalid at $I_2^{-1} > 0.3$ ($\lambda_1 < 1.33$), the deviation from the experimental results is not greater than about 7%. Also, for

$\lambda_1 < 1.33$, the values of $2W_2/G$ are less accurate than at larger extensions. Thus, if we assume as a first approximation that $2W_1$ is a constant and that $2W_2$ is dependent only on I_2, the strain energy function is represented approximately by:

$$W = G[0.3125(I_1 - 3) + 0.52 \ln(I_2/3)] \tag{26}$$

As I_1 and I_2 approach 3, Eq. (26) should approach $W = 2G(\lambda_1 - 1)^2$, the equation given by linear theory. Actually, Eq. (26) approaches $W = 1.943\ G(\lambda_1 - 1)^2$ in the limit of zero strain. This limiting form results because the data in Fig. 11 were fitted by a line of slope 1.04 instead of (3 x 0.375) = 1.125. However, the former slope gives the best over-all fit to the data, although it gives a somewhat incorrect result in the limit of zero strain.

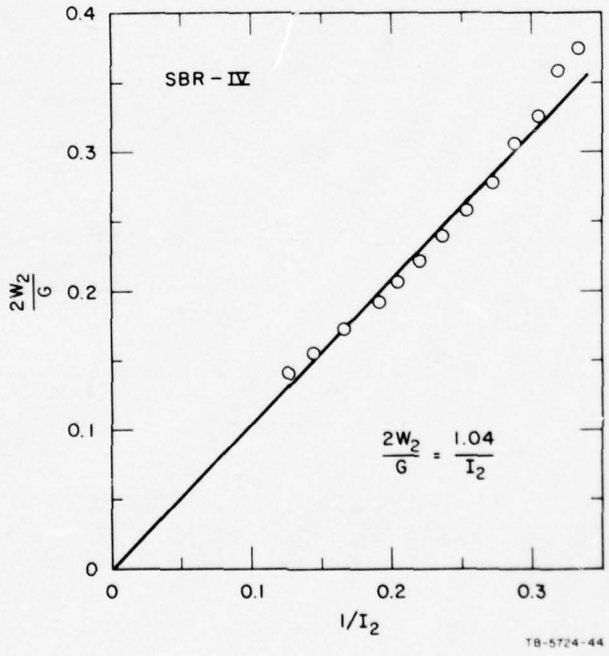

FIG. 11 PLOT OF $2W_2/G$ vs $1/I_2$

F. Comparison of Calculated and Experimental Uniaxial Tensile Data

From the uniaxial tensile data at five temperatures between 25 and 90°C, log $3\lambda\sigma/F(1)$ was derived and representative values at each temperature are shown by the points in Fig. 12. Within experimental error, $3\lambda\sigma/F(1)$ is temperature-independent.

The values of $2W_1/G$ and $2W_2/G$, given in Table V, were used in calculating uniaxial data and the results are shown by the solid curve in Fig. 12. The calculated values are somewhat less than the experimental values, although the greatest difference is less than 10%.

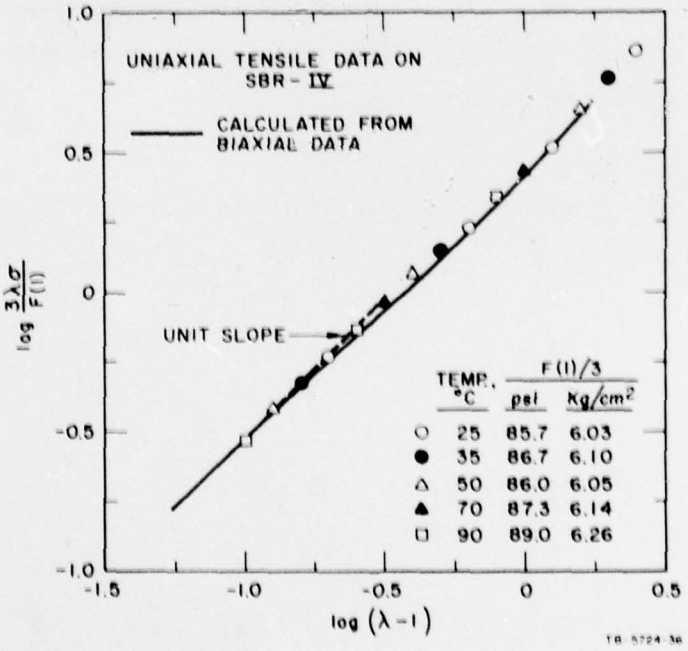

FIG. 12 UNIAXIAL TENSILE DATA (points) FROM TESTS AT CONSTANT EXTENSION RATES BETWEEN 25 AND 90°C COMPARED WITH RESULTS (solid curve) CALCULATED FROM BIAXIAL DATA

Equation (26) gives the following equation for stress-strain data in uniaxial tension:

$$\frac{\lambda\sigma}{G} = 0.625(\lambda^2 - \lambda^{-1}) + \frac{1.04\ (\lambda^3 - 1)}{2\lambda^3 + 1} \qquad (27)$$

Within the range $1.2 \leq \lambda \leq 2.2$, values of $\lambda\sigma/G$ from Eq. (27) agreed very closely (between about 0 and 2%) with those derived from the tabulated values of $2W_1/G$ and $2W_2/G$. For $2.2 < \lambda \leq 2.6$, the agreement was somewhat poorer (deviations up to 6%). However, this poorer agreement arises because Eq. (27) is based on the assumption that $2W_1/G$ is a constant whereas for $\lambda > 2.0$, $2W_1/G$ decreases somewhat with increasing λ_1 as indicated in Table V.

G. Attempt to Obtain Equilibrium Force-Temperature Data Under Biaxial Conditions

Attempts were made to determine the temperature dependence of $\bar{\sigma}_1$ and $\bar{\sigma}_2$ under equilibrium conditions at a series of axial extension ratios for $\lambda_2 = 1$. In principle, such data can be obtained by extending the cylindrical specimen to the desired value of λ_1, waiting until equilibrium is established, and then determining the stresses at a series of temperatures. (Once mechanical equilibrium is established, data can be obtained at other temperatures as soon as thermal equilibrium is established.) In practice, more than one day is required for SBR-IV to attain mechanical equilibrium at room temperature. During this period, the drift in the load cell and pressure transducer may be appreciable. Thus, equilibrium must be hastened by exposing a specimen to a higher temperature.

Two tests were made on SBR-IV specimens at $\lambda_2 = 1.0$ and $\lambda_2 \cong 1.25$. For each test, the stretched specimen was initially held at 60°C for about 2 hours; it is believed that equilibrium was achieved during this period. In the first test, the temperature was then decreased in increments of about 10°C to -40°C, and then the temperature was similarly increased. Thirty to forty minutes were allowed at each temperature to

establish thermal equilibrium, after which the axial force and the internal pressure were noted. Data obtained during the decrease and increase in temperature were in excellent agreement. However, during this test, no correction was made for the thermal contraction of apparatus components; thus, the distance between bench marks on the gage section of the specimen changed slightly with temperature.

In the second test, the crosshead of the Instron was adjusted at each temperature to maintain a constant distance between bench marks on the specimen. However, data obtained during the stepwise decrease in temperature were slightly higher than during the stepwise increase; the reason for this discrepancy is not known. Also, the axial force was lower by several percent at -40°C than observed in the first test; this difference resulted because the length of the specimen was maintained constant during the second test whereas it decreased slightly with decreasing temperature during the first test. Next, an attempt was made to obtain data at $\lambda_1 \cong 1.50$. However, after about 30 minutes at 50°C and before equilibrium was attained, the specimen ruptured. Another specimen was stretched to a $\lambda_1 = 1.50$ and then heated to 40°C. In this instance, the specimen ruptured after about 2.5 hours, again before equilibrium was established. It thus appears that equilibrium force-temperature data cannot be obtained on SBR-IV over an appreciable extension range owing to the propensity of specimens to rupture before equilibrium is attained.

Although precise data were not obtained at $\lambda = 1.25$, it is possible that the experimental procedure could be refined to give highly reliable data at this extension; a special effort would be required to obtain $\lambda_2 = 1.0$ precisely. (See Section II-D-2.) However, because of the desirability of obtaining data at a series of extensions, further work may possibly be done on a cylindrical specimen of either a natural rubber or silicone vulcanizate. The natural rubber vulcanizate should not rupture under the anticipated test conditions. Although the silicone vulcanizate may rupture at rather low extensions, equilibrium may be sensibly established prior to rupture and thus the desired data can possibly be obtained.

SECTION III

RUPTURE OF SBR-IV UNDER BIAXIAL AND UNIAXIAL TENSILE CONDITIONS

Figure 13, reproduced from the previous annual Technical Report,[4] shows rupture data from the biaxial tests on temperature-reduced plots of log $298\bar{\sigma}_{1b}/T\lambda_{1b}$, log $298\bar{\sigma}_{2b}/T$, and log λ_{1b} vs log $\dot{\lambda}_1 a_T$, where the subscript "b" indicates rupture. (The quantity $\bar{\sigma}_{1b}/\lambda_{1b}$ is the rupture stress, in the axial direction, based on the cross-sectional area of the unstressed specimen. For the circumferential stress $\bar{\sigma}_{2b}$, values based on the cross-sectional area of the stressed specimen are the same as those based on the deformed area.) Experimentally determined values of a_T gave, within experimental uncertainty, a straight line on a plot of log a_T vs $1/T$; the slope corresponded to an activation energy of 35 kcal. Values of log a_T from this plot were used to prepare reduced curves (Fig. 14) of the rupture data from uniaxial tests. (Individual values of the data are tabulated in Appendix IV of Ref. 4.)

Figure 15 shows a comparison of the uniaxial and biaxial rupture data. (The stress σ_{1b} is based on the cross-sectional area of unstressed specimens.) This figure shows that, within the experimental uncertainty, λ_{1b} is the same in both uniaxial and biaxial tension. If it is assumed that the three-chain network model discussed by Treloar[15] is valid, then it might possibly be expected that λ_{1b} will be the same under uniaxial and biaxial conditions. More precisely, the model predicts that $\lambda_m(\infty)$ will be the same under both test conditions. (The quantity $\lambda_m(\infty)$ is discussed in Appendix I.)

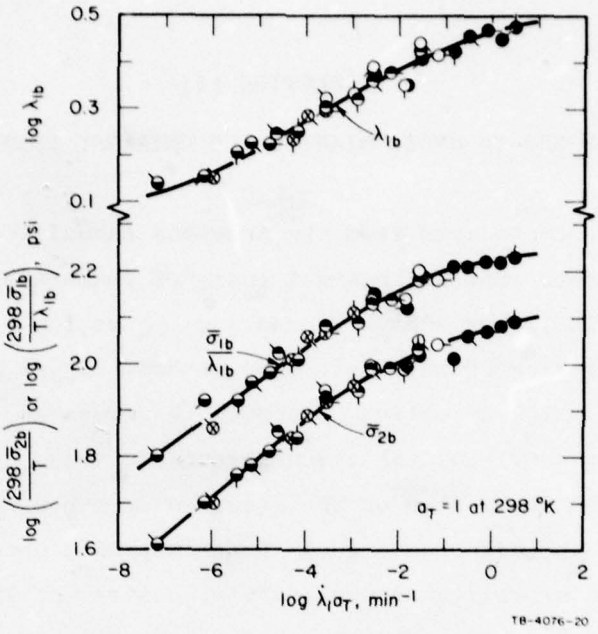

FIG. 13 RUPTURE DATA FROM BIAXIAL TESTS AT CONSTANT EXTENSION RATES ON SBR-IV BETWEEN 25 AND 90°C. Symbols and a_T values are same as used in Fig. 14. (Flags designate extension rate according to code shown in Fig. 9 of Ref. 4.)

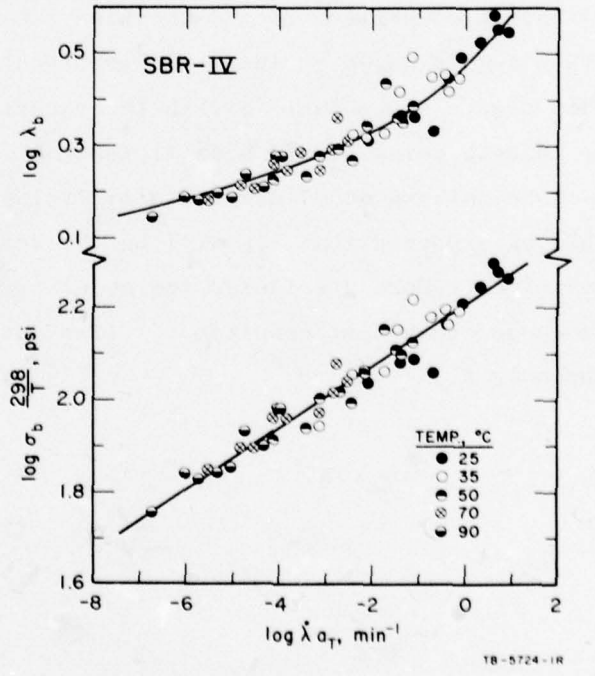

FIG. 14 RUPTURE DATA FROM UNIAXIAL TENSILE TESTS AT CONSTANT EXTENSION RATES ON SBR-IV BETWEEN 25 AND 90°C. Values of a_T given by an Arrhenius-Type plot for which ΔH_a = 35 kcal; a_T = 1 at 25°C.

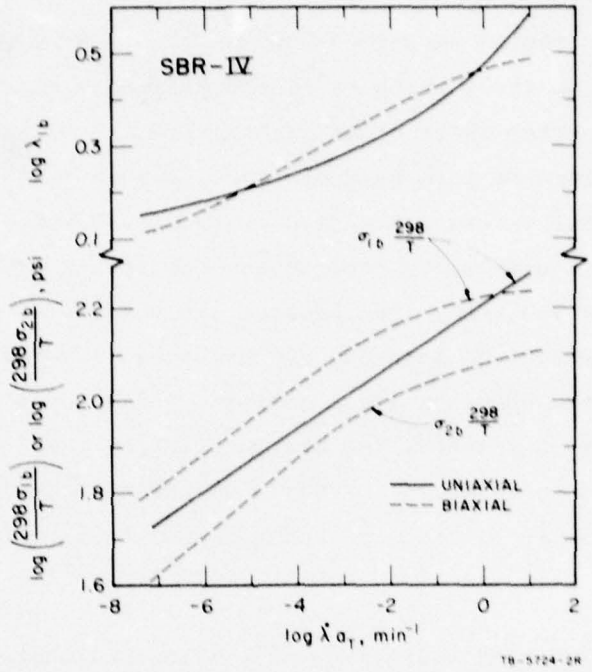

FIG. 15 COMPARISON OF RUPTURE DATA FROM UNIAXIAL AND BIAXIAL TENSILE TESTS ON SBR-IV. Curves are those from Figs. 13 and 14.

SECTION IV

BIAXIAL TENSILE PROPERTIES UNDER VARIOUS TYPES OF DEFORMATION FIELDS

A. Tests on Cylindrical Specimens

The biaxial tensile data presented in this report were obtained under a deformation field which is essentially pure shear. Data representing the properties under other deformation states can possibly be obtained by testing the thin-wall cylindrical specimens in different ways. For example, stress-relaxation tests can be made by mounting the ends of a specimen over end pieces whose diameter is greater than that of the unstressed specimen; the specimen can then be stretched in the axial direction while the internal gas pressure is regulated to maintain the diameter of the specimen equal to that of the end pieces. After the desired extension is reached, the decrease in the axial load and in the pressure required to maintain a fixed diameter can be monitored. Thus, it may be possible to obtain data under deformation fields for which $\lambda_2 > 1.0$.

Several preliminary tests were carried out following the procedure outlined above. For the tests, the end pieces had the diameter required to give a $\lambda_2 = 1.50$. At room temperature, the specimen was pressurized so that the specimen wall was parallel with the outside surfaces of the upper and lower end pieces and the specimen was stretched axially to a $\lambda_1 \cong 1.25$. However, when λ_1 was subsequently increased to about 1.50, the walls began to balloon, the size of the balloon increasing slowly with time. Next, a similar test at $\lambda_1 \cong 1.50$ was made at $-20^{\circ}C$. At this temperature, the specimen ballooned almost to rupture as soon as it was stretched axially. A similar type of instability was observed during tests at $-40^{\circ}C$ at $\lambda_2 = 1.0$ when λ_1 was greater than about 2.0.

The reason for the instability (ballooning in the gage section of a specimen) has been mentioned to us by Professor A. N. Gent, who has studied similar problems. For certain values of W_1 and W_2, a plot of

the pressure (P) inside the specimen against λ_1 will give a curve having a maximum and probably also a minimum at an extension greater than that at which the maximum occurs. This behavior signifies that λ_1 is a multi-valued function of P. Under such conditions, dimensional instability is expected because the specimen will tend to develop two extensions commensurate with the same internal pressure. In practice, factors other than W_1 and W_2 may affect the conditions for instability, e.g., end-effects and the nonhomogeneous stress across the wall of the cylinder possibly need to be considered.

To obtain a general idea about conditions that may be unstable, we assumed a Mooney-type of strain energy function and computed P vs λ_1 curves for different values of C_2/C_1 and for $\lambda_2 = 1.0$. When C_2/C_1 is greater than about 0.07, no maximum occurs. Based on studies[4] of the temperature dependence of C_1 and C_2 in uniaxial tension, it is expected that C_2/C_1 will decrease rapidly below some low temperature because of a rapid increase in C_1. Thus, for the SBR-IV specimens, the increased tendency for instability at -40°C may result from an increased W_1. (In the present context, W_1 and W_2 are identical to C_1 and C_2.) It is planned to carry out additional calculations of this type and especially to consider the conditions that may give instability when $\lambda_2 > 1.0$.

B. Apparatus for Tests in Equal Biaxial Tension

An objective of the present study is to determine the stress-strain characteristics and ultimate properties under different deformation fields. Experimental methods to obtain both types of data are difficult because the test specimen must be so designed that rupture does not occur near the edges where the specimen is gripped. (As discussed above, a thin-wall cylindrical specimen often cannot be tested when $\lambda_2 > 1$ because instability may develop in the gage section when the specimen is stretched in the axial direction.) One method which can be used to obtain both stress-strain and rupture data in equal biaxial tension ($\lambda_1 = \lambda_2 = \lambda_3^{-\frac{1}{2}}$) involves the inflation of a thin rubber sheet into a

balloon. To obtain data under such conditions, an apparatus, called a bubble tester, is being assembled.

Although several investigators[6,16-18] have obtained data by inflating either a rubber balloon or a thin rubber sheet, only a few comments about these studies will be made at this time. Treloar[18] studied in considerable detail the uniformity of the deformation over the surface of the bubble and found that the nonuniformity increased progressively with the distance away from the pole; the nonuniformity was particularly pronounced at high extensions. However, near the pole the deformation is uniform and the degree of deviation from uniformity depends on the particular form of the elastic strain energy, as shown by the theoretical analysis of Adkins and Rivlin.[19]

Some rupture data have been reported[16,17] and the macroscopic rupture mechanism has been considered by Treloar[18a] who observed that a specimen normally fragmented near the pole to give a large number of petal-shaped pieces. Because the bubble is thinnest at the poles, rupture will begin at or near this point and will be followed[18a] by cleavage of the sheet along radial lines which are parallel to the orientation direction of the network chains. For the several rubbers tested by Treloar, all gave a number of petals upon rupture, except for an SBR loaded with clay. Because a black-loaded SBR gave petals, Treloar concluded that crystallization has "no important bearing on the phenomenon, as SBR does not crystallize under any conditions."

The apparatus for the proposed study is shown in Fig. 16 and a schematic diagram is in Fig. 17. For a test, a rubber sheet is clamped between two circular metal rings (A) 4.0 inches in diameter; it is inflated into a bubble (B) by gas pressure. The height of the bubble as a function of time is controlled through the strain-gage sensor (C) and the associated servo-mechanism. To determine the radius of curvature and the extension ratio in the vicinity of the bubble's pole, concentric circles and radial marks will be inscribed on the undeformed sheet. The displacements of these fiducial lines will be determined, probably by a

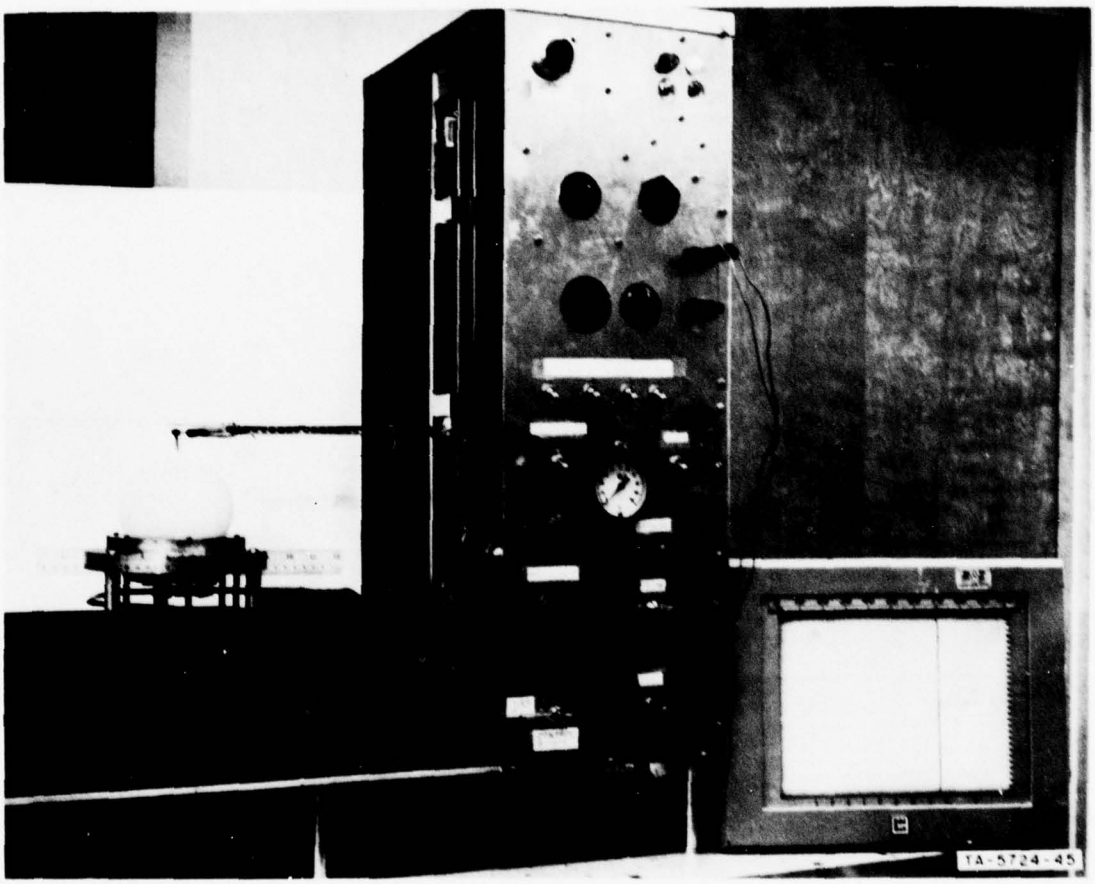

FIG. 16 PHOTOGRAPH OF APPARATUS (bubble tester) FOR STUDYING BEHAVIOR UNDER EQUAL BIAXIAL TENSION

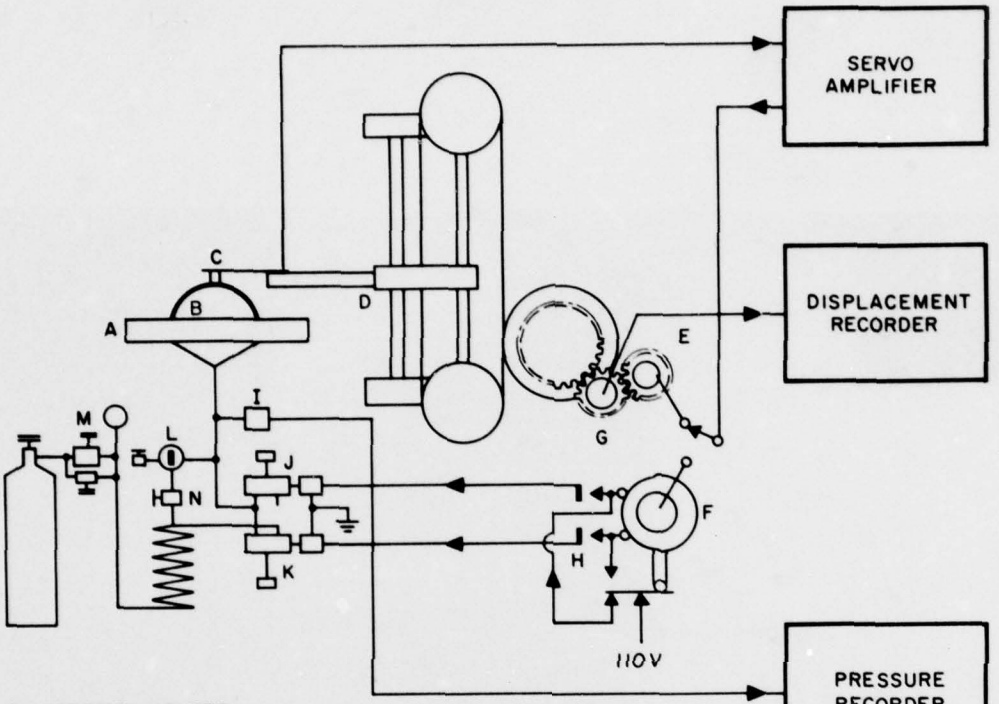

A—SPECIMEN HOLDER
B—SPECIMEN
C—STRAIN GAGE
D—FOLLOWER ARM
E—FOLLOWER MOTOR
F—PRESSURE MOTOR
G—ROTARY POTENTIOMETER
H—PRESSURE SWITCHES
I—PRESSURE TRANSDUCER
J—BLEED SOLENOID VALVE
K—PRESSURE SOLENOID VALVE
L—3-WAY VALVE
M—PRESSURE REGULATOR
N—FLOW CONTROL VALVE

TB-5724-25

FIG. 17 SCHEMATIC DIAGRAM OF APPARATUS (bubble tester) FOR STUDYING BEHAVIOR UNDER EQUAL BIAXIAL TENSION

photographic method, and the resulting data will be used in deriving the radius of curvature and the extension ratio. From the observed gas pressure, the initial thickness of the rubber sheet, and the radius of curvature we can derive the stress at the pole.

To make a relaxation test, the sensing device is locked in some predetermined position and gas pressure applied to inflate the rubber sheet into a bubble of the desired height. When the size of the bubble is sufficient to contact the sensing device, the resulting electrical output from the device activates the solenoid valves (J and K) to regulate the gas pressure to maintain a constant bubble height. During the ensuing stress relaxation, the pressure inside the bubble is monitored. When it is desired that the height of the bubble change continuously during a test, the sensing arm activates the servo-tracking device that provides a record of the height of the bubble as a function of time. It is planned, at least for the first tests, to control the height of the bubble as a function of time by manually regulating the pressure. For tests under a constant pressure, the servo-tracking device will give a time record of the bubble's height and photographic data will provide the extension ratio and the radius of curvature as a function of time.

To complete the apparatus, it will be necessary to develop a photographic procedure to determine the displacement of fiducial marks. In addition, a temperature-controlled cabinet, equipped with windows through which photographs can be taken, is needed. Work along these lines is in progress.

To date, only exploratory tests have been made to evaluate the operation of the servo-mechanism, and to verify that the clamping device will hold a specimen tightly and that rupture will occur near the pole of the balloon. For the latter, several sheets of natural rubber and one of a silicone rubber were inflated until rupture occurred. In each instance, rupture occurred in the vicinity of the pole. The natural rubber sheets fragmented explosively into numerous relatively small pieces, but the silicone sheet ruptured rather quietly to give a single, relatively

small fragment. Interestingly, the sizes of the silicone and natural rubber balloons at the instant of rupture were not too different, although the ultimate pressure inside the natural rubber balloon was severalfold greater.

SECTION V

SUMMARY

Stress-strain characteristics of an unfilled styrene-butadiene vulcanizate (SBR-IV) were determined under one type of biaxial tensile deformation at temperatures between -40 and 90°C and also under uniaxial tensile conditions between 25 and 90°C. The biaxial tensile data, which represent the response to essentially a pure shear deformation (i.e., $\lambda_2 = 1.0$ and $\lambda_1 = \lambda_3^{-1}$), were obtained by stretching thin-wall cylindrical specimens in the axial direction while internal gas pressure was controlled to maintain a constant outside diameter. Between 25 and 90°C, tests were made at constant extension rates (crosshead speeds between 0.02 and 20 inches per minute) whereas between -40 and 20°C, stress relaxation tests were made at axial extension ratios (λ_1) up to 2.5. Uniaxial tensile data were obtained by testing rings, cut from the thin-wall cylindrical specimens, at crosshead speeds between 0.02 and 20 inches per minute.

The biaxial data can be represented by:

$$\bar{\sigma}_1(\lambda_1, t) = 4G(t)\chi_1(\lambda_1)$$

$$\bar{\sigma}_2(\lambda_1, t) = 2G(t)\chi_2(\lambda_1)$$

where $\bar{\sigma}_1(\lambda_1, t)$ and $\bar{\sigma}_2(\lambda_1, t)$ are the stresses (each a function of λ_1 and the time t) in the axial and circumferential directions, respectively; G(t) is the small-deformation stress-relaxation modulus in shear; and $\chi_1(\lambda_1)$ and $\chi_2(\lambda_1)$ are functions only of λ_1. These functions become equal to $\lambda_1 - 1$ at sufficiently small deformations; under such conditions, the above equations represent the stress-relaxation characteristics of a linear viscoelastic material.

From the data, obtained at values of λ_1 up to about 2.5, $W_1/G(t) \equiv (\partial W/\partial I_1)/G(t)$ and $W_2/G(t) \equiv (\partial W/\partial I_2)/G(t)$ were evaluated. The quantity W, which is analogous to the elastic stored energy used in the

theory of finite equilibrium elasticity, is a function of t and the strain invarients $I_1 = \lambda_1^2 + \lambda_2^2 + \lambda_3^2$ and $I_2 = \lambda_1^2\lambda_2^2 + \lambda_1^2\lambda_3^2 + \lambda_2^2\lambda_3^2$. For the biaxial deformation field used in the present study, $I_1 = I_2 = \lambda_1^2 + \lambda_1^{-2} + 1$. In accordance with the above equations for $\bar{\sigma}_1(\lambda_1, t)$ and $\bar{\sigma}_2(\lambda_1, t)$, it was found that $W_1/G(t)$ and $W_2/G(t)$ are time- and temperature-independent, that $W_1/G(t)$ is sensibly constant for $I_1 < 5.5$ (i.e., $1 \leq \lambda_1 < 2.08$), and that $W_2/G(t)$ is a decreasing function of $I_1 = I_2$. Within the range $1 \leq \lambda_1 \leq 2.5$, the ratio W_2/W_1 decreased from about 0.60 to 0.25. Over the same range of λ_1, the ratio $\bar{\sigma}_1/\bar{\sigma}_2$ increased from 2.0 (the value given by classical elasticity theory) to about 3.5; for $\lambda_1 > 1.5$ the stress ratio is given by: $\bar{\sigma}_1/\bar{\sigma}_2 = 1.18\ \lambda_1 + 0.66$.

To a reasonably good approximation, $W(I_1, I_2, t)$ can be represented by:

$$W(I_1, I_2, t) = G(t)[0.3125(I_1 - 3) + 0.52 \ln (I_2/3)]$$

This equation appears to be valid approximately under the conditions for which $W_1/G(t)$ is a constant.

From the determined values of W_1 and W_2, as well as from the above equation for $W(I_1, I_2, t)$, uniaxial tensile data were calculated and found to agree quite closely with experimental data.

A comparison was made of rupture data obtained between 25 and 90°C in biaxial and uniaxial tension. Within the experimental uncertainty, the ultimate extension ratios in biaxial and uniaxial tension are identical at the same temperature and extension rate. However, the rupture stress in uniaxial tension lies between the axial and circumferential rupture stresses observed under biaxial tensile conditions.

An attempt was made to procure data by stretching the thin-wall specimens while the circumferential extension ratio λ_2 was maintained constant at a value of 1.5. Under such conditions, the specimens commonly ballooned in the gage section. This type of instability, which was also observed at -40°C when $\lambda_2 = 1.0$ and λ_1 was greater than about 2.0, occurs

REFERENCES

1. Smith, T.L., Mechanisms of Reversible and Irreversible Loss of Mechanical Properties of Elastomeric Vulcanizates Which Occur At Elevated Temperatures, Technical Documentary Report No. ASD-TDR 62-572, June 1962.

2. Smith, T.L., Ultimate Tensile Properties of Gum Vulcanizates and Their Temperature Dependence, Technical Documentary Report No. ASD-TDR 63-430, May 1963.

3. Smith, T.L., Characterization of Ultimate Tensile Properties of Elastomers, Technical Documentary Report No. ML-TDR-64-264, August, 1964.

4. Smith, T.L., Biaxial and Uniaxial Tensile Properties of Elastomers, Technical Report AFML-TR-65-356, March 1966.

5. Rivlin, R.S., "Large Elastic Deformations," Rheology Vol. I, Chapt. 10, F.R. Eirich, ed., Academic Press, New York, 1956. This chapter gives references to the original publications.

6. Rivlin, R.S. and Saunders, D.W., Phil. Trans. Roy. Soc. (London) A 243, 251 (1951).

7. Gent, A.N. and Thomas, A.G., J. Polymer Sci, 28, 625 (1958).

8. Hutchinson, W.D., Becker, G.W., and Landel, R.F., "Determination of the Stored Energy Function of Rubber-Like Materials," Bulletin of the 4th Meeting of the ICRPG Working Group on Mechanical Behavior, Chemical Propulsion Information Agency, Applied Physics Laboratory, Silver Spring, Maryland, CPIA Pub. No. 94U, Vol. 1, p. 141 (1965).

9. Becker, G.W., "On the Phenomenological Description of the Non-Linear Deformation Behavior of Rubberlike High Polymers," preprinted for and presented at the IUPAC International Symposium on Macromolecular Chemistry, Prague, 1965.

10. San Miguel, A., "On the Characterization of Multiaxial Data in Terms of the Strain Energy Concept," Bulletin of the 4th Meeting of the ICRPG Working Group on Mechanical Behavior, Chemical Propulsion Information Agency, Applied Physics Laboratory, Silver Spring, Maryland, CPIA Pub. No. 94U, Vol. 1, p. 169 (1965).

11. Bernstein, B., Kearsley, E., and Zapas, L., Trans. Soc. Rheology 7, 391 (1963); ibid., 9, Part 1, 27 (1965); J. Res. Nat'l. Bur. Stds. 68B, 103 (1964).

REFERENCES (Concluded)

12. Zapas, L.J. and Craft, T., J. Res. Nat'l. Bur. Stds. 69A, 541 (1965).

13. Halpin, J.C., J. Applied Phys. 36, 2975 (1965).

14. Smith, T.L., Trans. Soc. Rheology 6, 61 (1962).

15. Treloar, L.R.G., The Physics of Rubber Elasticity, 2nd ed., Clarendon Press, Oxford, 1958.

16. Sheppard, J.R. and Clapson, W.J., Ind. Eng. Chem. 24, 782 (1932).

17. Flint, C.F. and Naunton, W.J.S., Trans. Inst. Rubber Ind. 12, 367 (1937).

18. Treloar, L.R.G., (a) Trans. Inst. Rubber Ind. 19, 201 (1944); (b) Trans. Faraday Soc. 40, 59 (1944).

19. Adkins, J.E. and Rivlin, R.S., Phil. Trans. A 244, 505 (1952).

APPENDIX I

DEFORMATION AND FAILURE OF NONRIGID POLYMERIC MATERIALS

This appendix, an invited paper for presentation before the Division of Organic Coatings and Plastic Chemistry of the American Chemical Society at the Fall 1966 Meeting, has been preprinted by the Division in their preprint series Volume 26, Number 2, September 1966. Although portions of the paper are of a review nature (as requested by the organizers of the session at which the paper will be presented), other portions cover new work. The discussion Uniaxial Tensile Properties of Noncrystallizable Elastomers is the same as that submitted for the Informal Discussion Meeting on Nonlinear Viscoelastic Response of Polymeric Materials held at the Air Force Materials Laboratory, Wright-Patterson AFB, Ohio, on July 26-27, 1966.

APPENDIX I

DEFORMATION AND FAILURE OF NONRIGID POLYMERIC MATERIALS

Thor L. Smith
Stanford Research Institute
Menlo Park, California

INTRODUCTION

In many technological applications, a polymer experiences mechanical and thermal stresses which may cause either undue dimensional changes or rupture. To select the most reliable polymer for a specific need and to make an optimum engineering design, two types of information are needed. The first is the stress-strain-time-temperature relationships for the polymer, i.e., constitutive equations which represent the response characteristics of the material under the anticipated environmental conditions. (If the material is isotropic and is subjected to small deformations, constitutive equations can be formulated from experimental data in terms of the theory of linear viscoelasticity or, in some instances, of classical elasticity.) The second need is adequate failure criteria, i.e., a specification of the conditions under which rupture--or other undesirable instability--will occur. Under service conditions, the stress throughout a polymeric component is normally nonhomogeneous, giving regions of stress concentration in which rupture tends to occur under the existing combined (multiaxial) stress state. Thus, to predict failure, rupture data from tests under various multiaxial stress states are needed. Although few data of this type now exist, a significant amount of work is currently being directed toward establishing failure criteria and constitutive equations for representing response at deformations up to rupture.

To a high degree, the mechanical properties of a polymer are determined by its physical state. A polymer may be either amorphorous or semicrystalline, depending on its tendency to crystallize, on the temperature, and on its thermal and mechanical history. Above the glass

temperature, T_g, of an amorphous polymer, or above the melting point of a crystalline polymer, a crosslinked polymer is a rubberlike solid, and a noncrosslinked polymer is a liquid. (More precisely, the latter is an elastic liquid because under an applied stress, energy is both stored and dissipated.) The glass temperature (defined by the break-point in a plot of volume against temperature) is not a thermodynamic transition and is somewhat dependent on the cooling rate; a tenfold reduction in cooling rate decreases T_g by roughly $3^{\circ}C$. In the glassy state, the specific volume is a function of thermal history. In turn, thermal history affects to some degree the mechanical properties. Also, T_g as well as mechanical properties are sensitive to traces of soluble foreign materials.

The present discussion centers around the uniaxial tensile properties of amorphous polymers at temperatures above T_g. We first consider certain rheological properties of idealized materials and then the large deformation and ultimate (rupture) properties of elastomers in uniaxial tension. Although emphasis is placed on conventional elastomers, most of the principles outlined are applicable to highly crosslinked resins and noncrosslinked polymers at temperatures above T_g.

RHEOLOGICAL PROPERTIES OF MATERIALS WHICH EXHIBIT LINEAR RESPONSE

Rheology is a branch of mechanics devoted to studies of those properties of materials which determine their response to mechanical force. Commonly, Newtonian fluids and Hookean solids are excluded, because studies of such materials more properly lie in the fields of hydrodynamics and elasticity. Thus, rheology is concerned primarily with materials whose response characteristics depend on the stress-strain history, in addition to the instantaneous states of stress, deformation, and deformation rate.

To illustrate certain types of behavior, let us consider three idealized materials: a Hookean solid, a Newtonian liquid, and a linear

viscoelastic material. Further, let us suppose that each is subjected to a uniaxial tensile deformation which increases linearly with time, i.e., $\varepsilon = \dot{\varepsilon}t$, where ε, $\dot{\varepsilon}$, and t are strain, strain rate, and time, respectively. (This strain-time history is considered because the data discussed subsequently were obtained under such conditions.) For the three types of materials, we obtain:

Hookean Solid	$\sigma = E\varepsilon$	or	$\frac{\sigma}{\varepsilon} = E \equiv Et^{\circ}$
Newtonian Liquid	$\sigma = \eta_t \dot{\varepsilon}$	or	$\frac{\sigma}{\varepsilon} = \eta_t t^{-1}$
Linear Viscoelastic Material			$\frac{\sigma}{\varepsilon} = F(t)$

where E and η_t are the tensile modulus and tensile viscosity, both of which are independent of the magnitude of the deformation. The ratio σ/ε is inversely proportional to time for a Newtonian liquid and is independent of time (proportional to t°) for a Hookean solid. For a linear viscoelastic material, σ/ε is independent of the strain magnitude but is a function of time. The time function, F(t), called the constant-strain-rate modulus[1], gives a complete characterization (in principle) of the linear viscoelastic properties in uniaxial tension, provided it is known for $0 < t < \infty$. This modulus is related to the better known stress-relaxation modulus, E(t), by the equation:

$$E(t) = F(t) \left[1 + \frac{d \log F(t)}{d \log t} \right] \qquad (1)$$

Figure 1 illustrates the general features of F(t) and E(t) for a typical high molecular weight noncrosslinked polymer. At very short times (equivalent to conventional test conditions at a low temperature), the polymer exhibits glassy response; the modulus (about $10^{10.5}$ dynes/cm^2) is nearly time-independent. As time increases progressively, the modulus decreases to the so-called rubbery plateau at $10^{6.9}$ dynes/cm^2, attributed to a transient network of entangled chains. (If the polymer were crosslinked into a three-dimensional network by primary valence

bonds, than at long times the modulus would approach an equilibrium value, determined by the number of chemical crosslinks and permanently trapped physical entanglements.) At still longer times, the modulus decreases owing to viscous flow and the associated nonrecoverable deformation.

Figure 1 shows that the F(t) and E(t) curves are similar, except at very long times. In the rubber-to-glass transition zone, the greatest difference between E(t) and F(t) is a factor of about three. In the terminal relaxation region, F(t) is directly proportional to t^{-1}, whereas E(t) approaches a vertical asymptote.

The modulus F(t) is related to time by the proportionality $F(t) \propto t^{n(t)}$, where the time-dependent exponent n(t) lies on the range $-1 \leq n(t) \leq 0$. When $n(t) = 0$, the material shows Hookean behavior; when $n(t) = -1$, it exhibits Newtonian viscous flow. The exponent n(t) is a qualitative index of the relative amounts of energy dissipated and stored during the deformation. When $n(t) = 0$, the energy to deform a specimen is completely stored, but when $n(t) = -1$, the energy to maintain a constant deformation rate is completely dissipated as heat.

UNIAXIAL TENSILE PROPERTIES OF NONCRYSTALLIZABLE ELASTOMERS

Our starting point is the statistical theory of equilibrium rubber-like elasticity[2] which is envisioned applicable to a relatively perfect network structure formed from very long molecules, each molecule constituting many chains of high molecular weight in the final network. In the elementary development, the theory is based on the assumptions that the change in end-to-end separation of each network chain is directly related to the change in the macroscopic dimensions (an affine deformation) and that the free energy of each chain (predominantly entropic) is derivable from a Gaussian probability function. These assumptions lead directly to the elastic stored energy $W = \frac{G}{2}(\lambda_1^2 + \lambda_2^2 + \lambda_3^2 - 3)$, where G is the equilibrium shear modulus and

the λ's are the extension ratios* in the mutually perpendicular directions. For either uniaxial tension or compression, the stored energy gives:

$$\sigma = \frac{E_e}{3} (\lambda - \lambda^{-2}) \tag{2}$$

where σ is the stress based on the undeformed cross-sectional area and the equilibrium tensile modulus E_e equals 3G.

When the chains parallel to the stretch direction are highly extended, neither the Gaussian probability function nor the affine deformation assumption is valid. In one approach to the problem, Treloar[2] applies another probability function to the affine deformation (assumed) of a specific network model and obtains an equation which for uniaxial tension reduces to:

$$\sigma = G \left\{ \frac{\lambda_m(\infty)}{3} \mathcal{L}^{-1}\left[\lambda/\lambda_m(\infty)\right] - \frac{1}{\lambda^2} \right\} \tag{3}$$

where $\lambda_m(\infty)$ is the extension ratio (hypothetical) at which $d\sigma/d\lambda = \infty$ and $\mathcal{L}^{-1}(x)$ is the inverse Langevin function of $x \equiv \lambda/\lambda_m(\infty)$. Although this equation should not be considered quantitatively accurate, it predicts the correct shape of the stress-strain curve. When $\lambda/\lambda_m(\infty)$ is less than about 0.3, Eq. (3) reduces to Eq. (2).

Precise experimental tests of the statistical theory have shown several unexplained phenomena. First, equilibrium data are exceedingly difficult (commonly impossible) to obtain owing to a slow, yet persistent,

---

*For a specimen which is a rectangular parallelepiped, the extension ratios are $\lambda_1 = L/L_0$, $\lambda_2 = W/W_0$, and $\lambda_3 = T/T_0$, where L, W, and T are the length, width, and thickness of the deformed specimen and L_0, W_0, and T_0 are the dimension of the unstretched specimen. In the present discussion, the symbol λ is used in place of λ_1, where λ_1 is the extension ratio in the direction of a uniaxial stretch. The quantity $(\lambda-1)$, which equals $\Delta L/L_0$, is defined formally the same as the Cauchy strain ϵ. Because the volume of an elastomer is sensibly constant during a test, $\lambda_1\lambda_2\lambda_3 = 1$. Thus, the stress based on the cross-sectional area of a deformed specimen is $\lambda\sigma$.

relaxation or creep. For lightly crosslinked elastomers, the time dependence is normally more pronounced than for those more tightly crosslinked. Various studies of this phenomenon have been made; among the several proposed explanations, none has been generally accepted. The second unexplained phenomenon is that the stress (in uniaxial tension under near-equilibrium conditions) at intermediate extensions is somewhat less than predicted by Eq. (3), provided G is evaluated from data at small deformations. The third anomaly is the occurrence of rupture at small values of $\lambda/\lambda_m(\infty)$. At elevated temperatures, where equilibrium response is approached most closely, $\lambda_b/\lambda_m(\infty) \sim 0.2$, where λ_b is the extension ratio at break.

Certain general features of uniaxial tensile behavior are illustrated[3] in Fig. 2 by data on a Viton A-HV (hydrofluorocarbon) vulcanizate. The heavy curve (failure envelope) represents the locus of rupture data determined at various extension rates at eight temperatures between -5 and 230°C. The curves to the left of the envelope represent stress-strain data obtained at the same extension rate (data at two rates are shown at 55°C). The dashed curve on the envelope's right is the equilibrium curve derived indirectly as outlined below. The quantity $(\lambda_b)_{max}$ is the maximum observable ratio and $\lambda_m(\infty)$, defined above, is an estimate of the maximum extension ratio that would be observed under equilibrium conditions if rupture did not intervene.

We shall now consider data from uniaxial tensile tests at different extension rates and temperatures. (The approach outlined can also be applied to stress-relaxation and creep data.) The developed stress $\sigma(\lambda,t)$--a function of the extension ratio λ and the time t ($= (\lambda-1)/\dot{\lambda}$), where $\dot{\lambda}$ is the constant rate of extension)--can be decomposed into two functions as follows:

$$\sigma(\lambda,t) = F(t)\Gamma(\lambda,t) \qquad (4)$$

where $\Gamma(\lambda,t)$ is a function which approaches the Cauchy strain, $\lambda-1$, in the limit of zero extension. Thus, $F(t)$ is the modulus, discussed in the previous Section, and $\Gamma(\lambda,t)/(\lambda-1)$ is a measure of the deviation from linear response.

To evaluate $F(t)$ and $\Gamma(\lambda,t)$ from data at a series of constant extension rates, plots are first made of log σ vs log t, where the points along a single curve represent data at the same extension. An illustration is provided by Fig. 3 which shows data obtained on a Viton A-HV vulcanizate at 130°C. Because the lines are parallel, it follows that, within the experimental uncertainty, $\Gamma(\lambda,t)$ is independent of time over the range being considered. The negative slope shows that relaxation occurs continuously during a test at each extension rate. Thus, the curvature in a stress-strain curve is the result of two effects: (1) the continuous relaxation of stress; and (2) the inherent nonlinear relation between stress and strain.

To analyze the results further, values of stress and strain are read at a fixed value of time from the plots of log σ vs log t. (The resulting values are termed isochronal stress-strain data.) Commonly, 1-minute isochronal data are obtained and used to evaluate the 1-minute modulus, $F(1)$; this modulus can conveniently be obtained either from the initial slope of a plot of $\lambda\sigma$ vs $(\lambda-1)$ or from the position of the line of unit slope on a plot of log $\lambda\sigma$ vs log $(\lambda-1)$. After $F(1)$ has been obtained, 1-minute values of the strain function $\Gamma(\lambda,1)$ can be obtained from the relation $\sigma(\lambda,1)/F(1) = \Gamma(\lambda,1)$.

Over certain ranges of λ and t, the function $\Gamma(\lambda,t)$ is independent of time, as well as temperature,* and thus:

$$\frac{\sigma(\lambda,t)}{F(t)} = \Gamma(\lambda) = \frac{\sigma}{E_e} \qquad (5)$$

where σ/E_e is the ratio of the equilibrium stress to the equilibrium tensile modulus, E_e. Consequently, if $\Gamma(\lambda)$ is in fact time-independent and is available from large-deformation data, then the equilibrium

*In this discussion, it will be assumed that time-temperature superposition is applicable to data being considered. Thus, the phrase "range of time" will tacitly signify an equivalent temperature range.

stress-strain curve can be derived, provided E_e is known, at extensions above that at which rupture occurs under "equilibrium" test conditions.

It was noted some years ago by Guth and coworkers[4] and by Tobolsky and Andrews[5] that the equation $\sigma(\lambda,t) = E(t)\Gamma(\lambda)$ could often be used to represent stress-relaxation data. Several years ago, Eq. (5) was shown to be applicable for representing data[1], at extensions up to rupture, from tests at constant extension rate on an SBR vulcanizate at temperatures from -34 to 93°C. The utility of the equation $\sigma = E_e\Gamma(\lambda)$ was explicitly pointed out by Halpin[6,7] who showed that constant extension rate, stress relaxation, and creep data may (for certain materials) give sensibly the same $\Gamma(\lambda)$. (His data were on an SBR vulcanizate at temperatures down to -35°C and extensions up to nearly 700%.)

Let us now consider the conditions under which $\Gamma(\lambda,t)$--at least for some elastomers--might be expected to be time-independent as well as one reason for the function being time-dependent under other conditions. Following the approach of Halpin[7], we shall for expediency assume that the stress-strain curve is given approximately by Eq. (3) except that $\lambda_m(\infty)$ is replaced by a time-dependent extensibility $\lambda_m(t) \leq \lambda_m(\infty)$ and G is replaced by F(t)/3. This gives:

$$\frac{\sigma(\lambda,t)}{F(t)} \equiv \Gamma(\lambda,t) = \frac{1}{3}\left\{\frac{\lambda_m(t)}{3}\,\mathcal{L}^{-1}\left[\lambda/\lambda_m(t)\right] - \frac{1}{\lambda^2}\right\} \qquad (6)$$

To generalize somewhat and to indicate a graphical method for deriving $\lambda_m(t)$ from experimental data, Eq. (6) can be written in the form:

$$\left(\frac{3\lambda\sigma}{F(t)} + \frac{1}{\lambda}\right)\frac{1}{\lambda_m^2(t)} = \frac{\lambda}{3\lambda_m(t)}\,\mathcal{L}^{-1}\left[\lambda/\lambda_m(t)\right] \qquad (7a)$$

$$= f[\lambda/\lambda_m(t)] \qquad (7b)$$

where the function $f[\lambda/\lambda_m(t)]$ need not equal that on the right side of Eq. (7a). Because $\mathcal{L}^{-1}(x) = 3x + 9x^3/5 + \ldots$, the right side of Eq. (7a) reduces to λ (it becomes time independent) when $\lambda/\lambda_m(t)$ becomes less than

about 0.3. Equation (7) shows that $\lambda/\lambda_m(t)$ is a highly significant quantity and that account should be taken of $\lambda_m(t)$ in comparing stress-strain data for different materials.

One-minute isochronal data from constant extension rate tests on a Viton B vulcanizate are shown in Fig. 4 plotted as log $\Gamma(\lambda,1)$ vs log $(\lambda-1)$. Although the 1-minute modulus, F(1), increases from about 200 to 300 psi between 70 and -5°C, $\Gamma(\lambda,t)$ is sensibly independent of temperature (and also of time) at extensions up to about 100%; at intermediate extensions, the function is smaller than $(\lambda-\lambda^{-2})/3$, shown by the dotted line. At all extensions, $\Gamma(\lambda,t)$ is essentially temperature independent between 70 and 25°C; at large extensions below about 25°C, it depends on temperature because of the temperature dependence of $\lambda_m(t)$.

To obtain relative values of $\lambda_m(t)$, plots were made of log $[3\lambda\sigma/F(1) + \lambda^{-1}]$ vs log λ and these were superposed by shifting along a line of slope 2.0*; the shift distances gave $\lambda_m^\circ/\lambda_m$, where λ_m° and λ_m are the extensibilities at the reference temperature (25°C) and the other temperatures, respectively. The tabulated values of $\lambda_m^\circ/\lambda_m$ in Fig. 5 show that λ_m decreases by about 30% between 25 and -5°C. As Fig. 5 shows, data at different temperatures superpose quite well except at intermediate extensions where the points move upward with a temperature decrease. (This behavior arises because of the contribution of a term analogous to C_2 in the Mooney equation.) The ratio of the modulus to $\lambda_m^\circ/\lambda_m$ (tabulated in Fig. 5) is constant, and thus λ_m is inversely proportional to the modulus, 298F(1)/T. For other vulcanizates, it has been reported[7] that $\lambda_m(t) \propto [E(t)]^{-\frac{1}{2}}$. Undoubtedly, $\lambda_m(t)$ depends in a complex manner on network topology.

In recent years, considerable data has been obtained, usually covering three logarithmic decades of extension rate, on a variety of vulcanizates. (Normally, data were obtained at temperatures not less

---

*If Eq. (7b) is valid, then plots of data at different temperatures (or times) must superpose when shifted in this manner.

than 20°C above T_g.) For many vulcanizates under all conditions at which $\lambda_m(t)$ is constant, isothermal data at extensions up to rupture can be represented by Eq. (5), $\sigma(\lambda,t) = F(t)\Gamma(\lambda)$. However, for certain vulcanizates (commonly those very lightly crosslinked), the equation is applicable only for $\lambda < \lambda_c \ll \lambda_m(t)$, where λ_c is seldom less than about 2.0.

A somewhat extreme example of the temperature dependence (and thus time dependence) of $\Gamma(\lambda,t)$ is provided by data (Fig. 6) on a lightly crosslinked Viton A-HV vulcanizate. The extensibility $\lambda_m(t)$ decreases below 25°C as shown by the curves which represent data at -5, 10, and 25°C. Because rupture occurred at relatively low elongations at 130 and 230°C, $\lambda_m(t)$ cannot be estimated, although it is expected to be either equal to or greater than at 25°C. The reason for values of $\Gamma(\lambda,t)$ at 130 and 230°C being greater than at 25°C is not known.

A more typical example of the temperature dependence of $\Gamma(\lambda,t)$ is provided by data (Fig. 7) for a crosslinked poly(methylmethacrylate) polymer in its rubbery state. For this polymer, $\Gamma(\lambda,t)$ increases progressively as the temperature decreases from 165 to 125°C. (This behavior is similar to that found by Halpin[8] in studies of lightly crosslinked styrene-butadiene rubber vulcanizates; he attributed the behavior to a nonaffine migration of network junction points at high extensions and to the progressive increase in this phenomenon as the temperature is increased.) The relatively rapid increase in $\Gamma(\lambda,t)$ at high extensions at 125 and 135°C results from finite extensibility effects, i.e., λ begins to approach $\lambda_m(t)$, as illustrated more clearly by the data in Fig. 4.

ULTIMATE PROPERTIES OF ELASTOMERS IN UNIAXIAL TENSION

The ultimate properties in uniaxial tension are the tensile strength, σ_b, and the associated ultimate extension ratio, λ_b. These quantities are strongly dependent on the temperature and the stress-strain history. Although σ_b and $\lambda_b - 1$ are relatively small at elevated

temperatures (150-250°C above T_g), these quantities increase by factors of about 30 and 10, respectively, as the temperature is decreased. Concomitantly, the modulus for some elastomers shows little or no increase, whereas for others it may increase severalfold. When the temperature is reduced further, the breaking elongation, $(\lambda_b-1)100$, decreases, but the tensile strength continues to increase; the modulus, however, increases rapidly and approaches the value for glassy (plastic) polymers.

Before the ultimate properties of different elastomers can be compared, it is necessary to characterize in some detail the time and temperature dependence of these properties. Two methods are available; both necessitate the determination of rupture data over broad ranges of temperature and extension rate. (Equally acceptable for characterization are rupture data from creep or, within a certain temperature range, stress-relaxation tests.) Ultimate property data are notoriously non-reproducible, and thus under given test conditions ultimate properties can be specified precisely only by statistically treating data from repetitive tests. On the other hand, it is usually of greater value to obtain data at a large number of extension rates than to statistically define the ultimate properties at a single or even several extension rates; the resulting data can be represented by a smoothed curve which gives a reasonably good representation of the average or most probable values at extension rates in the range being considered.

The first method of characterizing ultimate properties is based on the application of time-temperature superposition to interrelate rupture data at different temperatures and extension rates[9]. The superposition procedure, which appears to be applicable--at least approximately--to data on amorphous elastomers, leads to composite curves which show the dependence of the tensile strength on either the temperature-reduced extension rate, $\dot{\lambda}a_T$, or the temperature-reduced time-to-break, t_b/a_T. (The quantity a_T is the temperature-dependent shift factor[10] commonly used in superposing curves which represent mechanical property data at various temperatures to obtain a composite plot.) Such curves, along with a_T as a function of temperature, enable the ultimate properties to be predicted over wide ranges of extension rate and temperature.

Because the curves depend on stress-strain history, they are not suitable for predicting when rupture will occur under an arbitrary stress-time or strain-time history.

The second method is in terms of a failure envelope[11], often represented by a plot of log $\sigma_b T_\circ / T$ vs log $(\lambda_b - 1)$. (A typical failure envelope is shown in Fig. 8.) Provided time-temperature superposition is applicable, values of σ_b and λ_b give a single curve (envelope) which is independent of time (extension rate) and temperature; either a decrease in temperature or an increase in extension rate merely shifts a point, representing rupture data, counterclockwise around the envelope. Although the failure envelope may depend somewhat on stress-strain history[12] the dependence is apparently slight unless the histories are grossly dissimilar, e.g., that associated with a cyclic stress as compared with a monotonically nondecreasing stress.

The failure envelope shows clearly the maximum observable extension ratio, $(\lambda_b)_{max}$. At conventional extension rates, $(\lambda_b)_{max}$ is observed at a temperature which, depending on the elastomer, is roughly 30-55°C above the glass temperature. At lower test temperatures, or at the equivalently higher extension rates, rupture data commonly do not superpose to provide a smooth extension of the curve defined by data at higher temperatures or lower extension rates; thus, under these conditions, ultimate properties can probably be characterized only roughly by a failure envelope or the composite curves which show the time-dependence of the data.

Two important quantities defined by a failure envelope are $(\lambda_b)_{max}$ and the associated tensile strength $(\sigma_b)_{max}$. The maximum extensibility is quite sensitive to network topology and depends on crosslink density according to the approximate relation $(\lambda_b)_{max} \propto M_c^n$, where M_c is the average molecular weight of effective network chains and n should equal 0.5 if the network deforms affinely. In practice, however, n may be significantly greater[3] than 0.5, a reflection of the increased extensibility which results from the nonaffine deformation of the network. The true tensile strength, $(\lambda_b \sigma_b)_{max}$, for the elastomers thus far

studied is roughly 10^4 psi, within a factor of 2 to 4. Thus, as a first approximation $(\sigma_b)_{max} \cong 10^4 \ (\lambda_b)^{-1}_{max}$.

The characterization of the ultimate properties for various elastomers enables their properties to be compared and their endurance under different test conditions to be predicted. However, the available data on noncrystallizable elastomers show that their properties are remarkably similar, provided proper account is taken of differences in glass temperature and crosslink density. An increase (or decrease) in T_g shifts the composite curves, which represent the time dependence of the ultimate properties, toward a higher (or lower) temperature, owing to the change in time-scale for molecular rearrangements. A change in crosslink density has a strong effect on the ultimate elongation, although under many conditions (especially low or high temperature) the effect on tensile strength often is rather small.

It is reasonable to assume that different elastomers are in corresponding states when the test conditions are such that rupture occurs at $(\lambda_b)_{max}$. When $(\lambda_b)/(\lambda_b)_{max}$ and $\log \sigma_b T_o/T$ are plotted against $\log t_b/(t_b)_{max}$, where $(t_b)_{max}$ is the rupture time (temperature reduced) at which $(\lambda_b)_{max}$ is observed, the curves from data on a variety of elastomers not only are found to be quite similar in shape but also to lie rather close together, as shown in Fig. 9. Thus, a change in chemical structure, and even in crosslink density, gives primarily a change in $(t_b)_{max}$ and $(\lambda_b)_{max}$.

The stress-strain and ultimate properties of crystallizable elastomers are modified markedly when stress-induced crystallization occurs. The change in stress-strain properties is the composite effect of stress decay associated with crystallization and the subsequent increase in the slope of the stress-strain curve caused by the reinforcing action of the hard crystalline phase. The ultimate properties are affected because crystallization probably begins preferentially in the vicinity of an incipient crack and thus inhibits its formation and growth. Consequently, under many test conditions, a specimen can be stretched to a high degree, and thus can sustain a high stress, without

rupture occurring. When the test conditions are progressively changed so that the extent of crystallization increases, the ultimate elongation progressively decreases[13,14].

Reinforcing filler in a crystallizable elastomer may modify the conditions under which stress-induced crystallization occurs, and in this way, alter the ultimate properties. In a noncrystallizable elastomer, filler decreases the rate of certain relaxation processes and thus the high-strength regime is displaced toward a higher temperature[15]. However, at elevated temperatures, filler has a relatively small effect[14,15], the increase in tensile strength being about the same as that in the modulus; the modulus increase may be nearly that represented by the Guth-Smallwood equation.

Although a comparison of the macroscopic properties of various elastomers can provide useful relations between ultimate properties and network structure, an understanding of rupture can only result from studies of the rupture mechanism and a delineation of the factors which affect this process. Rupture entails the formation of a crack whose growth slowly accelerates until a high-speed terminal velocity is reached. The new surface area formed during the slow-growth stage may indeed be quite small, and thus the rupture process can appear to occur suddenly. However, there is considerable evidence that crack growth may occur during a significant fraction of the entire test period.

The rupture theories of Bueche and Halpin[16] and of Knauss[17] provide relations between ultimate and viscoelastic properties. In the Bueche-Halpin theory, a viscoelastic function--commonly the creep compliance--is related to the ultimate properties through two parameters; one includes the critical stress (or the related critical elongation) for rupture at the crack tip; and the other is a parameter which is the ratio of the total time before high-speed crack growth to the rupture time for each successive filament at the crack tip. In the theory of Knauss, the relation is formulated in terms of a time-dependent stored energy; when the product of the crack length and the stored energy attains a critical value, catastrophic crack propagation ensues.

ACKNOWLEDGMENTS

The author wishes to acknowledge the Air Force Materials Laboratory at Wright-Patterson Air Force Base for their sponsorship of research which lead to the majority of the results in this paper. Also, certain of the data were obtained during the conduct of research for the National Aeronautics and Space Administration on Contract NASr-49(13).

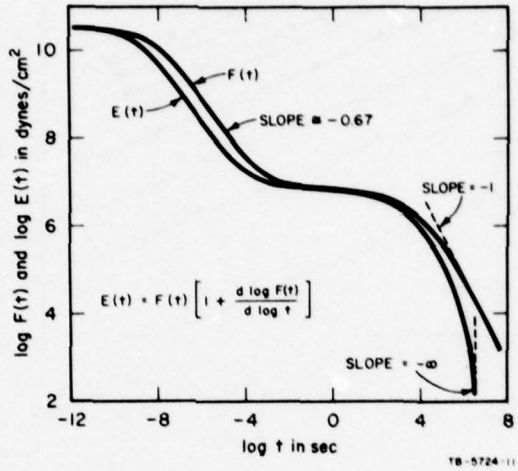

FIGURE I-1

ILLUSTRATION OF THE TIME DEPENDENCE OF THE STRESS-RELAXATION MODULUS, E(t), AND THE CONSTANT-STRAIN-RATE MODULUS, F(t), FOR A HIGH MOLECULAR WEIGHT *NONCROSSLINKED POLYMER*

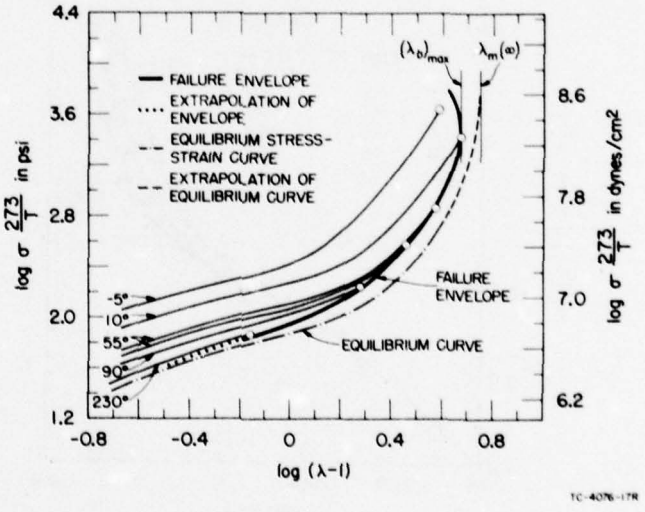

FIGURE I-2

CHARACTERISTIC FEATURES OF STRESS-STRAIN CURVES AND FAILURE ENVELOPE. Data are for Viton A-HV (hydrofluorocarbon) vulcanizate (A-6).

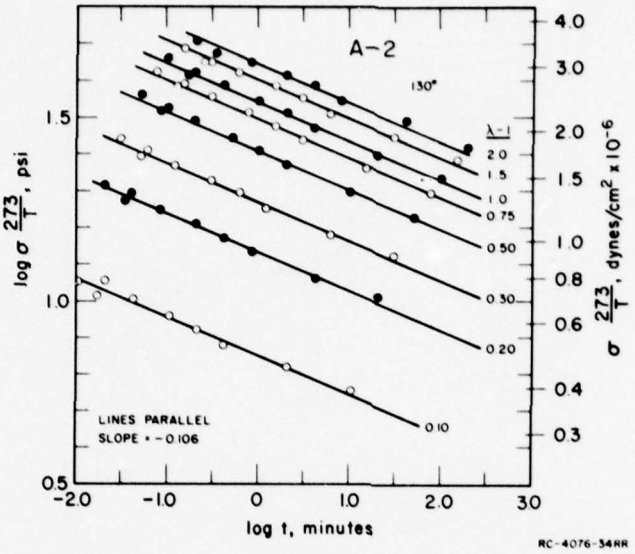

FIGURE I-3

STRESS-STRAIN DATA FROM TESTS AT CONSTANT EXTENSION RATES ON A VITON A-HV (A-2) VULCANIZATE. Lines connect points representing data at constant values of strain, $\lambda-1$.

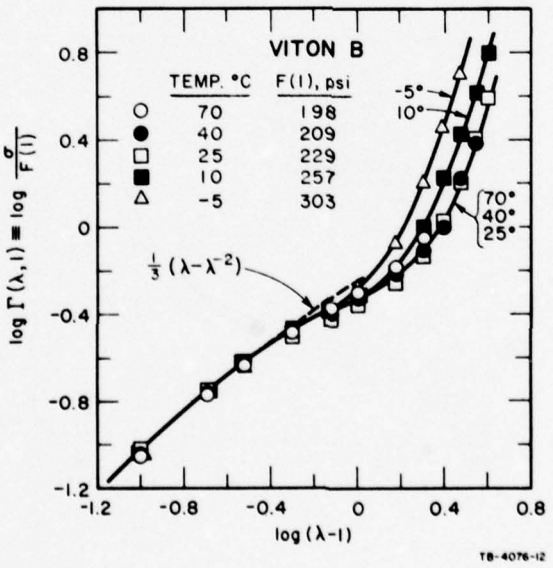

FIGURE I-4

TEMPERATURE DEPENDENCE OF STRAIN FUNCTION $\Gamma(\lambda,t)$ FROM 1-MINUTE DATA ON VITON B VULCANIZATE

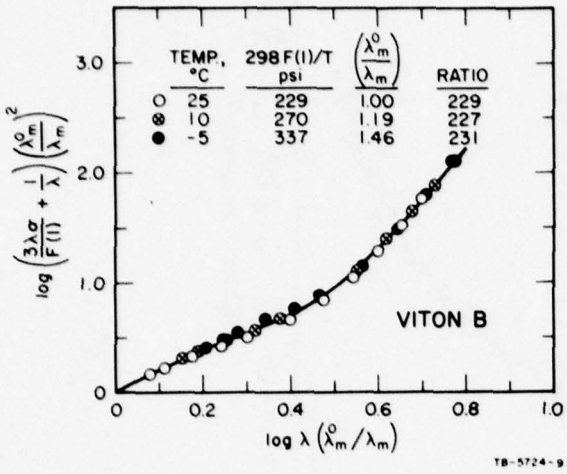

FIGURE 1-5

ONE-MINUTE DATA ON VITON B VULCANIZATE PLOTTED IN A MANNER TO ACCOUNT FOR THE TEMPERATURE DEPENDENCE OF THE MAXIMUM EXTENSIBILITY

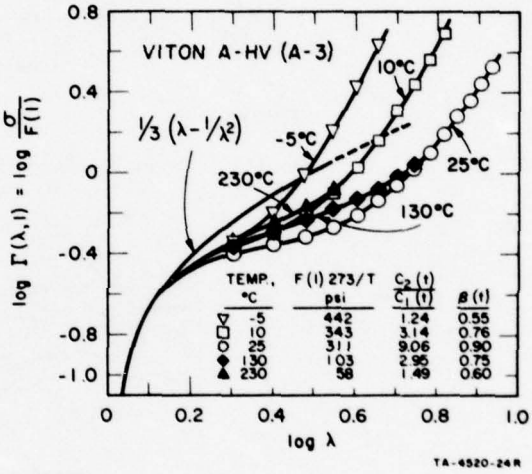

FIGURE 1-6

STRAIN FUNCTION $\Gamma(\lambda, t)$ FROM 1-MINUTE DATA ON VITON A-HV VULCANIZATE (A-3) AT SELECTED TEMPERATURES BETWEEN -5 AND 230 °C

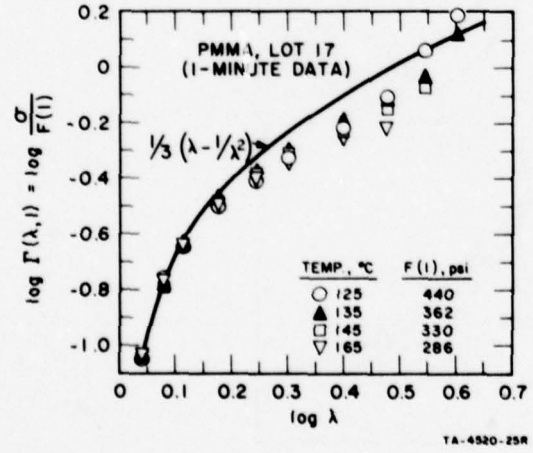

FIGURE 1-7

STRAIN FUNCTION $\Gamma(\lambda,t)$ FROM 1-MINUTE DATA ON A CROSSLINKED POLY(METHYL-METHACRYLATE) RUBBER AT SEVERAL TEMPERATURES

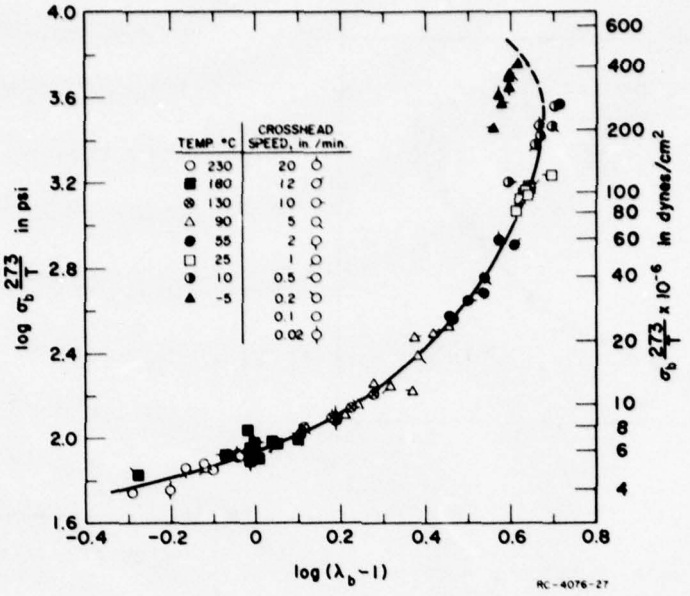

FIGURE 1-8

FAILURE ENVELOPE FOR A VITON A-HV (A-6) VULCANIZATE

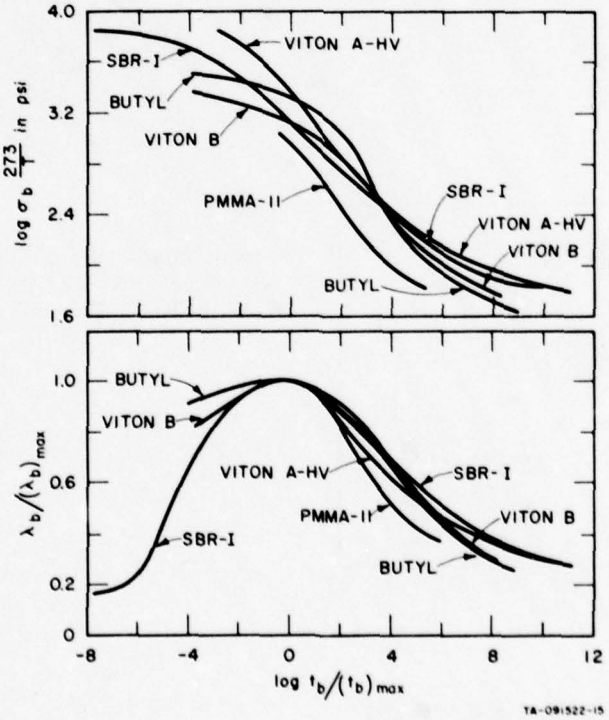

FIGURE 1-9

COMPARISON OF TIME DEPENDENCE OF σ_b AND λ_b FOR DIFFERENT ELASTOMERS; $(t_b)_{max}$ IS THE TIME-TO-BREAK WHICH CORRESPONDS TO $(\lambda_b)_{max}$

REFERENCES

1. Smith, T.L., Trans. Soc. Rheology 6, 61 (1962).

2. Treloar, L.R.G., The Physics of Rubber Elasticity, 2nd ed., Clarendon Press, Oxford, 1958.

3. Smith, T.L. and Frederick, J.E., J. Appl. Phys. 36, 2996 (1965).

4. Guth, E., Wack, P.E., and Anthony, R.L., J. Appl. Phys. 17, 347 (1946).

5. Tobolsky, A.V. and Andrews, R.D., J. Chem. Phys. 13, 3 (1945).

6. Halpin, J.C., Polymer Letters 2, 959 (1964).

7. Halpin, J.C., J. Appl. Phys. 36, 2975 (1965).

8. Halpin, J.C., J. Polymer Sci. (in publication).

9. Smith, T.L., J. Polymer Sci. 32, 99 (1958).

10. Ferry, J.D., Viscoelastic Properties of Polymers, John Wiley and Sons, Inc., New York, 1961.

11. Smith, T.L., J. Polymer Sci. A1, 3597 (1963).

12. Smith, T.L., Polymer Engineering and Science 5, 270 (1965).

13. Smith, T.L., J. Appl. Phys. 35, 27 (1964).

14. Smith, T.L., unpublished results.

15. Halpin, J.C. and Bueche, F., J. Appl. Phys. 35, 3142 (1964).

16. (a) Halpin, J.C., Rubber Reviews, of Rubber Chem. and Tech. 38, 1007 (1965); J. Appl. Phys. 35, 3133 (1964). (b) Bueche, F. and Halpin, J.C., J. Appl. Phys. 35, 36 (1964).

17. Knauss, W., "The Time-Dependent Fracture of Viscoelastic Materials," presented at the International Conference on Fracture, Sendai, Japan, 1965.

APPENDIX II

TIME AND TEMPERATURE DEPENDENCE OF STRESS-STRAIN DATA FOR AN UNFILLED NATURAL RUBBER VULCANIZATE

Several years ago, the stress-strain behavior and the ultimate properties in uniaxial tension were determined[1-3] on an unfilled vulcanizate of natural rubber at 8 to 10 crosshead speeds at temperatures between -55 and 150°C. (At 150°C some chemical degradation occurred during the test periods and thus no detailed analysis was made of the data.) The time (strain rate) and temperature dependence of the ultimate tensile properties have been discussed[1, 3, 4] and a preliminary--and thus somewhat approximate--analysis of the stress-strain data has also been presented.[1] In this Appendix, a more extensive and somewhat more refined analysis of the stress-strain data is presented.

When an elastomer is stretched, the decreased configurational entropy of the network increases the tendency of the chains to crystallize. This is illustrated by the rapid crystallization in a stretched natural rubber vulcanizate, in contrast to the slow crystallization in the unstretched vulcanizate. The crystallization rate and the morphology of the resulting crystalline phase depend on temperature, strain, and elapsed time, as well as on the mechanical and thermal histories. Thus, an adequate description of the mechanical properties of crystallizable elastomers would require a quantitative understanding not only of crystallization kinetics and crystal morphology but also of the effect of the crystalline phase on the response characteristics of the remaining amorphous matrix. Because relatively little is known about the interplay of such factors, present understanding of large deformation properties of crystallizable elastomers is largely qualitative.

During the crystallization of a specimen at a fixed extension, the stress decreases and, under certain conditions, becomes less than zero, i.e., it becomes compressive. When specimens are tested at a series of

constant extension rates and temperatures, the stress-strain data are particularly difficult to interpret because of two competitive processes: (1) stress relaxation caused by crystallization; (2) reinforcement provided by the hard crystalline regions dispersed in the rubbery matrix which reduces the extensibility of the vulcanizate and causes a marked increase in stress, at a given elongation, over that for the completely amorphous vulcanizate.

In considering the stress-strain data obtained at different extension rates on the natural rubber vulcanizate, we shall discuss first the time dependence of the stress at extensions below those at which crystallization occurs and then at the higher extensions at which the data reflect the crystallization. Following this discussion, 1-minute isochronal stress-strain data at various temperatures are considered primarily in terms of the change in maximum extensibility effected by differing states of crystallinity.

A. Time Dependence of Stress-Strain Data

The stress-strain curves from tests at the different extension rates were analyzed by the method which was adopted several years ago.[5] Plots were first made of log σ vs log t, where each curve results from data at the same value of the extension ratio λ. (The tensile stress σ is based on the cross-sectional area of the unstressed specimen and the time t equals $(\lambda-1)/\dot{\lambda}$, where $\dot{\lambda}$ is extension rate.) At temperatures above -5°C, the data gave lines of zero slope, except at large values of λ, i.e., those at which the vulcanizate is in a semicrystalline state. This behavior shows that the data represent, within the experimental accuracy, equilibrium response. At and below -5°C, relaxation occurred during the test periods owing to viscoelastic effects. This behavior is illustrated in Fig. II-1 which shows data at $\lambda = 1.2$ at temperatures between -5 and -45°C. At -5 and -20°C, relaxation occurred to a relatively small extent and only at the shorter times.

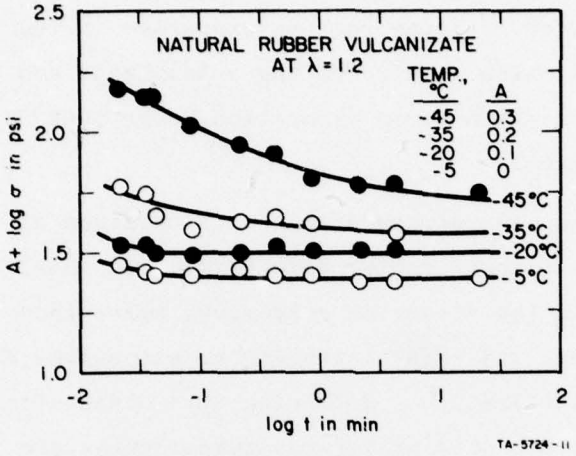

FIG. II-1 EFFECT OF TEMPERATURE AND TIME ON THE STRESS IN SPECIMENS OF A NATURAL RUBBER VULCANIZATE AT λ = 1.2. (Data are from tests at a series of constant extension rates.)

At high extensions, the behavior is complex because of the competition between relaxation caused by crystallization and the increased stress from reinforcement by the relatively hard crystalline phase. This behavior is illustrated by the data in Fig. II-2 which are λ = 7.0 and at selected temperatures between 100 and -45°C. The data show the following: above 10°C, the stress decreases with time whereas at 10°C the stress is sensibly time-independent; at -5 and -20°C, the stress increases with time, although at -45°C, the stress first decreases and then increases with time. These dissimilar effects result because the degree and rate of crystallization are dependent on the temperature, extension, and extension rate.

Various studies[6], as well as thermodynamic considerations, show that at higher temperatures crystallization begins at a higher extension and proceeds to a smaller extent than at lower temperatures. Thus, the decrease in stress with time (i.e., with decreasing extension rate) at 25 and 100°C is consistent with the assumption that the degree of

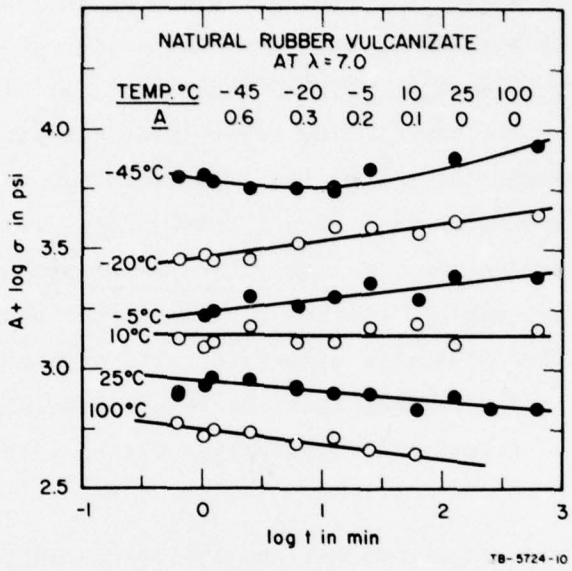

FIG. II-2 EFFECT OF TEMPERATURE AND TIME ON THE STRESS IN SPECIMENS OF A NATURAL RUBBER VULCANIZATE AT $\lambda = 7.0$. (Data are from tests at a series of constant extension rates.)

crystallization increases with time and that the reinforcement produced by the crystalline phase, which forms largely at a high extension and in a relatively small amount, is not sufficient to offset the stress decay associated with crystallization. This viewpoint is reasonable, although it seemingly is in disagreement with results (discussed by Treloar[6]) from a study of the birefringence of stretched raw rubber; the birefringence data showed that at 25°C crystallization was nearly complete immediately after extending the specimen and that at 50°C crystallization was sensibly complete in the time required (a few seconds) to extend the specimen. However, these dissimilar observations can probably be explained by noting that the ingredients added during the preparation of a vulcanizate normally increase the time required for crystallization.

The increase in stress with time at -5 and -20°C can be explained by assuming that the degree of crystallization again increases with time and that now a major portion of the crystallization occurs at extension ratios considerably below 7.0. (These assumptions are in agreement with results discussed by Treloar.[6]) The crystalline material which forms at $\lambda < 7.0$ acts to augment the stress required to attain a $\lambda = 7.0$. Thus, if the degree of crystallization at a λ below 7.0 is relatively large and is an increasing function of time, then the stress at $\lambda = 7.0$ should also be an increasing function of time. This behavior can result because the relaxation in stress associated with crystallization at extensions below $\lambda = 7.0$ is less than the reinforcing effect produced by the relatively large fraction of crystalline material which forms during the test.

At 10°C, the two effects cancel and the stress is time-independent. The initial decrease in stress at -45°C may result in part from a relatively long induction period for the beginning of crystallization (possibly little crystallization occurs at extensions markedly below $\lambda = 7.0$); stress decay may also reflect viscoelastic stress relaxation. The increase in stress at times greater than about 10 minutes undoubtedly results from the same processes that give a stress increase at -5 and -20°C. These presumably occur because the test period is sufficiently long so that considerable crystallization occurs before an extension ratio of 7.0 is reached.

A qualitative indication of the time dependence of the stress at extension ratios other than 1.2 and 7.0 is given in Table II-1.

Table II-1

STRESS-TIME BEHAVIOR OF NATURAL RUBBER VULCANIZATE
AT FIXED EXTENSIONS SHOWN BY DATA
FROM TESTS AT CONSTANT EXTENSION RATES

Temperature °C	Approximate Ranges of λ for Indicated Behavior		
	$(d\sigma/dt) = 0$	$(d\sigma/dt) < 0$	$(d\sigma/dt) > 0$
100	< 5.5	> 5.5	--
80	< 5.5	> 5.5	--
60	< 5.5	> 5.5	--
40*	--	--	--
25	≤ 2.0	> 2.0	--
10	all λ	--	--
- 5	--	--	≥ 5.5
-20	--	--	> 4.0
-35	--	--	≥ 5.0
-45**	--	< 4.5**	> 4.5**

*Data are anomalous; $d\sigma/dt = 0$, within experimental uncertainty, at all λ.

**For $\lambda > 4.5$, behavior is the same as illustrated in Fig. II-2.

B. Isochronal Stress-Strain Data

One-minute values of the stress, read from the plots of log σ vs log t, were used to construct plots of log $\lambda\sigma$ vs log $(\lambda-1)$. Data between -45 and 120°C and for elongations up to about 100% gave a precise fit to straight lines of unit slope. From these lines, values of the 1-minute modulus, F(1), were obtained and are tabulated in Table II-2. Although these values differ only slightly from those obtained from the previous analysis[1] of the data, they are tabulated here for convenience and because they are probably somewhat more reliable.

Table II-2

VALUES OF THE 1-MINUTE MODULUS, F(1),
FOR NATURAL RUBBER VULCANIZATE

Temperature °C	log F(1) psi	F(1) psi
120	2.380	240
110	2.276	189
100	2.270	186
90	2.270	186
80	2.252	179
60	2.255	180
40	2.207	161
25	2.208	161
10	2.200	159
- 5	2.173	149
-20	2.190	155
-35	2.195	157
-45	2.302	200

Figure II-3 shows data at selected temperatures on plots of $\sigma(1)/F(1)$ vs $\lambda-1$, where $\sigma(1)$ is the 1-minute value of the stress. These curves show clearly the change in the stress-strain curve which results from a variation of the degree of crystallinity with temperature. The temperature dependence of log $\sigma(1)/F(1)$ at $\lambda = 7.0$ is shown in Fig. II-4. Because the points representing data at 110 and 120°C lie somewhat below the dotted line, it is likely that some chemical degradation occurred during the test period at these elevated temperatures, although the 1-minute modulus at 120°C (Table II-2) appears to be unduly high instead of low as should be found if degradation occurred. The curve in Fig. II-4 has a maximum at -35°C, an indication that the degree

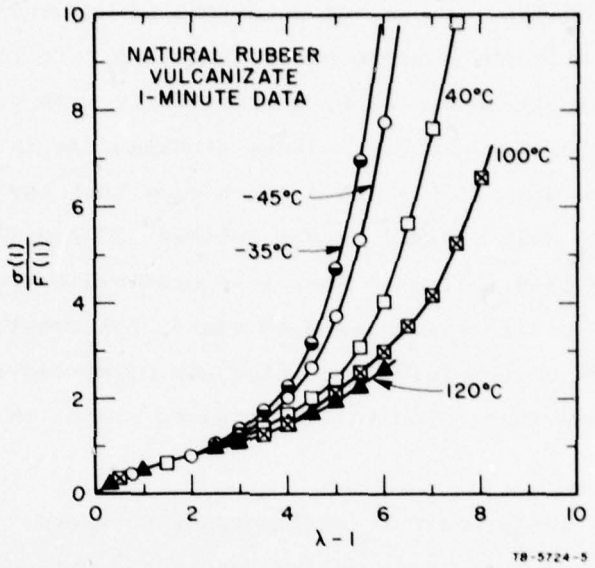

FIG. II-3 DATA AT VARIOUS TEMPERATURES FOR THE NATURAL RUBBER VULCANIZATE SHOWN BY PLOTS OF $\sigma(1)/F(1)$ vs. $\lambda-1$, WHERE $\sigma(1)$ AND $F(1)$ ARE 1-MINUTE VALUES OF THE STRESS AND MODULUS, RESPECTIVELY

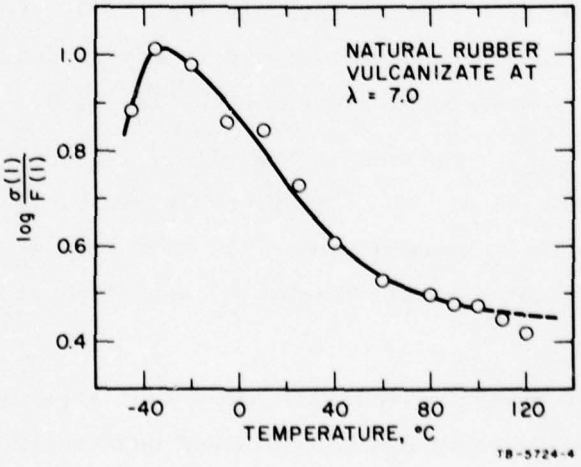

FIG. II-4 DATA ON NATURAL RUBBER VULCANIZATE AT $\lambda = 7.0$ SHOWN BY PLOT OF log $\sigma(1)/F(1)$ vs TEMPERATURE

of crystallization is a maximum at this temperature. Russell,[7] who studied the crystallization rate of a variety of natural rubber vulcanizates, found that the maximum crystallization rate in the unstretched vulcanizates occurs at about -26°C, in conformity with results reported by Wood[8] for unvulcanized rubber. These findings are in rather close agreement with the data in Fig. II-4 which show that the stress at $\lambda = 7.0$ changes by only a small amount between -20 and -35°C. The plots in Figs. II-3 and II-4 indicated that less crystallization occurs at -45°C than at -35°C. In the unstressed state, the crystallization rate of natural rubber[9] is sensibly zero below -50°C; stress-relaxation data[10] at $\lambda = 1.5$ indicate that, even in the stressed state, the rate is very low at -50°C.

As discussed in Appendix I, an important parameter that affects stress-strain behavior at large extensions is the maximum extensibility, $\lambda_m(t)$. This quantity, which is a function of time and thus also of temperature, is the extension ratio at which $d\sigma/d\lambda = \infty$, where σ and λ are isochronal values at time t. The 1-minute isochronal data for natural rubber at various temperatures were superposed, following the method outlined in Appendix I, to obtain the ratio $\lambda_m^\circ/\lambda_m$, where λ_m° is the maximum extensibility at 100°C and λ_m the value at temperature T. The resulting composite plot is shown in Fig. II-5. (Data at all temperatures between 100 and -45°C could be superposed, although data at only selected temperatures are shown in Fig. II-5.

The ratio $\lambda_m^\circ/\lambda_m$, tabulated in Fig. II-5, is seen to increase from unity at 100°C to 1.43 at -20°C; it probably achieves a maximum at -35°C. However, this ratio is somewhat lower at -45°C than at -20°C, undoubtedly because the degree of crystallization is lower than at a somewhat higher temperature.

Although the present discussion shows that stress-strain data on a natural rubber vulcanizate can be explained qualitatively, the extent of crystallinity, and thus the stress-strain behavior, depends on the mechanical and thermal histories. Thus, the results represented in Fig. II-5 cannot be used to predict mechanical response under arbitrarily selected test conditions.

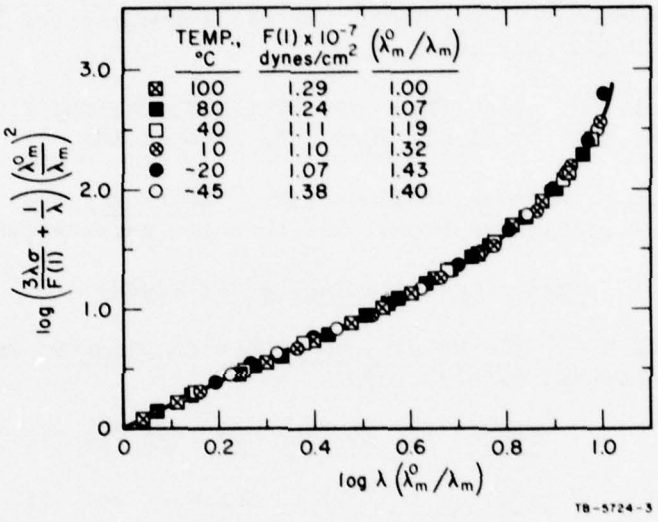

FIG. II-5 ONE-MINUTE DATA ON NATURAL RUBBER VULCANIZATE PLOTTED IN A MANNER TO ACCOUNT FOR THE TEMPERATURE DEPENDENCE OF THE MAXIMUM EXTENSIBILITY λ_m

REFERENCES

1. Smith, T.L., Mechanisms of Reversible and Irreversible Loss of Mechanical Properties of Elastomeric Vulcanizates Which Occur at Elevated Temperatures, Technical Documentary Report No. ASD-TDR 62-572, June 1962.

2. Smith, T.L., Ultimate Tensile Properties of Gum Vulcanizates and Their Temperature Dependence, Technical Documentary Report No. ASD-TDR 63-430, May 1963.

3. Smith, T.L., J. Appl. Phys. 35, 27 (1964); Smith, T.L. and Frederick, J.E., J. Appl. Phys. 36, 2996 (1965).

4. Smith, T.L., "Rupture of Elastomers," Rheology, Vol. IV, F. R. Eirich, ed., Academic Press, New York (in publication).

5. Smith, T.L., Trans. Soc. Rheology 6, 61 (1962).

6. Treloar, L.R.G., The Physics of Rubber Elasticity, 2nd ed., Clarendon Press, Oxford, 1958.

7. Russell, E. W., Trans. Faraday Soc. 47, 539 (1951).

8. Wood, L.A., in Advances in Colloid Science, Vol. II, Interscience, 1946, p. 57.

9. Wood, L.A. and Bekkedahl, N., J. Appl. Phys. 17, 362 (1946).

10. Tobolsky, A.V. and Brown, G.M., J. Polymer Sci. 17, 547 (1955).

APPENDIX III

COMPOUNDING RECIPE FOR STYRENE-BUTADIENE VULCANIZATE, SBR-IV

The ingredients in the styrene-butadiene vulcanizate, SBR-IV, and the cure conditions are given below. The specimens, prepared at the Air Force Materials Laboratory, were thin-wall cylindrical specimens whose dimensions are: inside diameter, 1.50 inches; wall thickness (nominal), 0.05 inch; gage length, 6.0 inches; length of filets between gage section and oversized end sections, 0.75 inch; and the length and wall thickness of end sections are 1.25 inches and 0.15 inch, respectively. A schematic diagram and photograph of a specimen are given elsewhere.* Although the nominal wall thickness of the gage section is 0.05 inch, the best determined value is 0.048 inch.

Ingredients	Quantity
Firestone 1502 SBR	100
Zinc Oxide	4
Methyl Tuads	4
Stearic Acid	1
Altax (MBTS)	1

Formulation cured for 60 minutes at 300° F.

*Smith, T.L., Biaxial and Uniaxial Tensile Properties of Elastomers, Technical Report AFML-TR-65-356, March 1966.

UNCLASSIFIED
Security Classification

DOCUMENT CONTROL DATA - R&D
(Security classification of title, body of abstract and indexing annotation must be entered when the overall report is classified)

1. ORIGINATING ACTIVITY (Corporate author)	2a. REPORT SECURITY CLASSIFICATION
Stanford Research Institute Menlo Park, California	UNCLASSIFIED
	2b. GROUP

3. REPORT TITLE

VISCOELASTIC AND FAILURE PROPERTIES IN BIAXIAL AND UNIAXIAL TENSION

4. DESCRIPTIVE NOTES *(Type of report and inclusive dates)*
Annual Technical Report, 24 August 1965 to 23 August 1966

5. AUTHOR(S) *(Last name, first name, initial)*

Smith, Thor L. and Frederick, J. E.

6. REPORT DATE	7a. TOTAL NO. OF PAGES	7b. NO. OF REFS
December 1966	94	46

8a. CONTRACT OR GRANT NO.	9a. ORIGINATOR'S REPORT NUMBER(S)
AF 33(615)3248	AFML-TR-65-356, Part II
b. PROJECT NO. 7342	
c. Task 734202	9b. OTHER REPORT NO(S) *(Any other numbers that may be assigned this report)*
d.	SRI Project No. 5724

10. AVAILABILITY/LIMITATION NOTICES

Approved for public release; distribution unlimited.

11. SUPPLEMENTARY NOTES	12. SPONSORING MILITARY ACTIVITY
	Air Force Materials Laboratory, Research & Technology Division, AF Systems Command, Wright-Patterson AFB, Ohio 45433

13. ABSTRACT

An unfilled styrene-butadiene vulcanizate was studied under a biaxial tensile deformation (essentially, pure shear) by stretching thin-wall cylindrical specimens axially while internal gas pressure was controlled to maintain a constant outside diameter. Between 25 and 90°C, specimens were stretched at crosshead speeds between 0.02 and 20 inches per minute; between -40 and 20°C, stress-relaxation measurements were made. From the data, at axial extension ratios λ_1 up to about 2.5, $W_1/G(t) \equiv (\partial W/\partial I_1)/G(t)$ and $W_2/G(t) \equiv (\partial W/\partial I_2)/G(t)$ were evaluated. W is analogous to the elastic stored energy; $I_1 = I_2 = \lambda_1^2 + \lambda_1^{-2} + 1$ are the strain invariants; and G(t) is the small-deformation stress-relaxation modulus in simple shear. It was found that $W_1/G(t)$ and $W_2/G(t)$ are time- and temperature-independent, that $W_1/G(t)$ is sensibly constant for $I_1 < 5.5$ (i.e., $\lambda_1 < 2.08$), and that $W_2/G(t)$ is a decreasing function of $I_1 = I_2$. From the results, uniaxial tensile data were calculated and found to agree with experimental data. (U)

A comparison of rupture data between 25 and 90°C in biaxial and uniaxial tension showed that the ultimate extension ratios in biaxial and uniaxial tension are sensibly identical (at the same temperature and extension rate) but that the uniaxial rupture stress lies between the axial and circumferential rupture stresses under the biaxial tensile conditions. (U)

A discussion is also given of the large deformation and ultimate properties of noncrystallizable vulcanizates in uniaxial tension and of the large deformation properties of a natural rubber vulcanizate. (U)

DD FORM 1 JAN 64 1473

UNCLASSIFIED
Security Classification

14. KEY WORDS	LINK A		LINK B		LINK C	
	ROLE	WT	ROLE	WT	ROLE	WT
Styrene-Butadiene Vulcanizate Nonlinear Viscoelastic Properties Biaxial (pure shear) and Uniaxial Tension Stress Relaxation Constant Extension Rate Rupture in Biaxial and Uniaxial Tension Noncrystallizable Vulcanizates Natural Rubber Vulcanizate						

INSTRUCTIONS

1. ORIGINATING ACTIVITY: Enter the name and address of the contractor, subcontractor, grantee, Department of Defense activity or other organization *(corporate author)* issuing the report.

2a. REPORT SECURITY CLASSIFICATION: Enter the overall security classification of the report. Indicate whether "Restricted Data" is included. Marking is to be in accordance with appropriate security regulations.

2b. GROUP: Automatic downgrading is specified in DoD Directive 5200.10 and Armed Forces Industrial Manual. Enter the group number. Also, when applicable, show that optional markings have been used for Group 3 and Group 4 as authorized.

3. REPORT TITLE: Enter the complete report title in all capital letters. Titles in all cases should be unclassified. If a meaningful title cannot be selected without classification, show title classification in all capitals in parenthesis immediately following the title.

4. DESCRIPTIVE NOTES: If appropriate, enter the type of report, e.g., interim, progress, summary, annual, or final. Give the inclusive dates when a specific reporting period is covered.

5. AUTHOR(S): Enter the name(s) of author(s) as shown on or in the report. Enter last name, first name, middle initial. If military, show rank and branch of service. The name of the principal author is an absolute minimum requirement.

6. REPORT DATE: Enter the date of the report as day, month, year; or month, year. If more than one date appears on the report, use date of publication.

7a. TOTAL NUMBER OF PAGES: The total page count should follow normal pagination procedures, i.e., enter the number of pages containing information.

7b. NUMBER OF REFERENCES: Enter the total number of references cited in the report.

8a. CONTRACT OR GRANT NUMBER: If appropriate, enter the applicable number of the contract or grant under which the report was written.

8b, 8c, & 8d. PROJECT NUMBER: Enter the appropriate military department identification, such as project number, subproject number, system numbers, task number, etc.

9a. ORIGINATOR'S REPORT NUMBER(S): Enter the official report number by which the document will be identified and controlled by the originating activity. This number must be unique to this report.

9b. OTHER REPORT NUMBER(S): If the report has been assigned any other report numbers *(either by the originator or by the sponsor)*, also enter this number(s).

10. AVAILABILITY/LIMITATION NOTICES: Enter any limitations on further dissemination of the report, other than those imposed by security classification, using standard statements such as:

(1) "Qualified requesters may obtain copies of this report from DDC."

(2) "Foreign announcement and dissemination of this report by DDC is not authorized."

(3) "U. S. Government agencies may obtain copies of this report directly from DDC. Other qualified DDC users shall request through _____."

(4) "U. S. military agencies may obtain copies of this report directly from DDC. Other qualified users shall request through _____."

(5) "All distribution of this report is controlled. Qualified DDC users shall request through _____."

If the report has been furnished to the Office of Technical Services, Department of Commerce, for sale to the public, indicate this fact and enter the price, if known.

11. SUPPLEMENTARY NOTES: Use for additional explanatory notes.

12. SPONSORING MILITARY ACTIVITY: Enter the name of the departmental project office or laboratory sponsoring *(paying for)* the research and development. Include address.

13. ABSTRACT: Enter an abstract giving a brief and factual summary of the document indicative of the report, even though it may also appear elsewhere in the body of the technical report. If additional space is required, a continuation sheet shall be attached.

It is highly desirable that the abstract of classified reports be unclassified. Each paragraph of the abstract shall end with an indication of the military security classification of the information in the paragraph, represented as *(TS), (S), (C), or (U)*.

There is no limitation on the length of the abstract. However, the suggested length is from 150 to 225 words.

14. KEY WORDS: Key words are technically meaningful terms or short phrases that characterize a report and may be used as index entries for cataloging the report. Key words must be selected so that no security classification is required. Identifiers, such as equipment model designation, trade name, military project code name, geographic location, may be used as key words but will be followed by an indication of technical context. The assignment of links, roles, and weights is optional.